Journal of
Computer Science & Systems Biology

Zhu et al., J Comput Sci Syst Biol 2015, 8:1
DOI: 10.4172/jcsb.1000166

Research Article Open Access

An Integrated Method for Detecting Micro RNA Target Proteins through Reverse-phase Protein Arrays

Jiawen Zhu[1], Song Wu[1] and Jie Yang[2]*

[1]*Department of Applied Mathematics and Statistics, Stony Brook University, Stony Brook, NY 11790, USA*
[2]*Department of Preventive Medicine, Stony Brook University, Stony Brook, NY 11790, USA*

Abstract

Objective: Understanding functions of microRNAs (or miRNAs), particularly their effects on protein degradation, is biologically important. Emerging technologies, including the reverse- phase protein array (RPPA) for quantifying protein concentration and RNA-seq for quantifying miRNA expression, provide a unique opportunity to study miRNA-protein regulatory mechanisms. One naïve way to analyze such data is to directly examine the correlation between the raw miRNA measurements and protein concentrations estimated from RPPA. However, the uncertainty associated with protein concentration estimates is ignored, which may lead to less accurate results and significant power loss.

Methods: We propose an integrated nonlinear hierarchical model for detecting miRNA targets through original RPPA intensity data. This model is fitted within a maximum likelihood framework and the correlation test between miRNA and protein is assessed using Wald tests. We compare this model and the simple method through extensive simulation studies and a real dataset from the Cancer Genome Atlas (TCGA) project.

Results: This integrated method is shown to have consistently higher power than the simple method, especially when sample sizes are limited and when the RPPA intensity levels are close to the boundaries of imaging limits.

Conclusions: Our proposed method is powerful in detecting miRNA's protein target through RPPA. We recommend this method in practice.

Keywords: MicroRNA; Reverse-phase Protein Arrays; Nonlinear mixed model; Micro RNA target

Introduction

MicroRNA (miRNA) is a set of small, non-coding RNA molecules that can post-transcriptionally regulate a broad range of gene expression in both plants and animals. They have been suggested to be involved in many important biological processes, such as normal physiological development and disease onsets. In the past decade, many efforts have been put to search for the miRNA targets [1]. Although our understanding on some miRNAs has been dramatically improved, as of today, the targets of many others remain largely unknown. Therefore, powerful methods for efficient detection of miRNA targets are still in great need.

In general, miRNA regulates the expression of its target genes through two mechanisms–mRNA degradation or translation inhibition. That is, if a miRNA and its target gene can complement extensively, the miRNA-mRNA target may form a double-strand RNA (dsRNA) structure, after which, the mRNA can be cleaved and degraded to lower the mRNA expression and subsequently protein expression [2,3]. On the other hand, if a miRNA and its target can only complement partially, the target mRNA will not be directly degraded but its translation may be repressed [4,5]. So, in both mechanisms, the total protein level relating to the miRNA targets would be reduced, resulting in their functional losses.

Based on the phenomenon that the sequences of miRNAs and their target genes complement to each other, or at least partially, one way of the miRNA target identification is through in silico prediction. Several software tools have been developed for such purpose, each with its own unique feature. For example, miRanda scored the likelihoods of mRNA down-regulation according to a regression model that is trained on sequence and contextual features of the predicted miRNA::mRNA duplex [6], and Target Scan studies on the miRNA::mRNA duplex interactions according to a thermodynamics-based modeling and comparative sequence analysis [7]. Based on these computational tools, several databases with predicted miRNA targets have been generated (microRNA.org and targetscan.org). However, one major limitation is that they all suffer from large percentage of false positives, which hinder their practical usage.

Another popular way to determine the miRNA targets is through experimental data by measuring downstream effects of miRNAs. Since miRNAs can induce protein reduction via both functional mechanisms, protein expression seems to be the right mark. However, due to difficulties in high- throughput quantification of protein expression but relative ease in that of mRNA, conventionally, scanning of the miRNA targets is mainly through testing negative correlations between miRNAs and mRNAs. For example, high-throughput techniques, such as miRNA and mRNA gene microarray, can be applied to measure their expression levels, and then the correlations analyses can be conducted subsequently to filter out miRNA-mRNA pairs that show significant negative correlations as potential candidates for further analyses [8]. More recently, with the advent and rapid advance of sequencing techniques, the miRNA sequencing (miRNA-seq) and RNA sequencing (RNA-seq) platforms have become more and more

***Corresponding author:** Jie Yang, Department of Preventive Medicine, Stony Brook University, Stony Brook, NY 11790, USA, Tel: 631-444-2191; Fax: +1 631-444-7525; E-mail: jie.yang@stonybrookmedicine.edu

Received November 03, 2014; **Accepted** November 18, 2014; **Published** January 01, 2015

Citation: Zhu J, Wu S, Yang J (2015) An Integrated Method for Detecting Micro RNA Target Proteins through Reverse-phase Protein Arrays. J Comput Sci Syst Biol 8: 012-033. doi:10.4172/jcsb.1000166

popular for the quantification of the miRNA and RNA expressions. The main drawback for the miRNA/mRNA correlation analyses is that they can only identify miRNA targets that may change at mRNA levels, but is determined to fail for those modulated through translation inhibition. Therefore, miRNA/mRNA correlation analysis is only able to find partial targets of miRNAs.

It is only until recently that a new technology, called the reverse phase protein array (RPPA) or protein lysate array has been developed to simultaneously quantify the protein expression in a large sample cohort [9]. In contrast to the usual array design that quantifies expression levels of multiple genes in one sample, the RPPA measures the protein expression levels of many samples on one array. Usually, a 2-fold serial dilution of samples is used to avoid signal saturation for very high protein concentration. Since the RPPA data are measured through image signals, which are characterized by background noises at the low end and saturation signals at the high end, a sigmoid-like response curve model has been used to estimate protein concentration [10,11]. Additionally, some flexible nonparametric joint sample models have also been proposed [12]. In principle, we can directly use the protein concentrations estimated from these methods to correlate with miRNA expression for miRNA target identification. However, in this case, the uncertainties associated with the protein concentration estimates are ignored, leading to less accurate and less powerful inference.

In this article, we propose an integrated hierarchical model to detect miRNA targets based on protein expression data measured by the recently emerged RPPA and high throughput miRNA- seq data. Extensive Monte Carlo simulations have been performed to examine the performance of our proposed model under different scenarios. This model was further applied to a real dataset from TCGA to demonstrate its practical use.

Methods

PPA

To quantify the protein expression on a RPPA array, a sigmoidal model is commonly assumed to describe the relationship between the intensity level and the protein concentration with additive error [10,13]:

$$y_{ij} = g(x_i, l_j, \beta) = \beta_1 + \frac{\beta_2}{1+2^{-\beta_3(x_i+l_j)}} + \varepsilon_{ij} \quad (1)$$

where y_{ij} is the gray-level intensity from sample i at jth dilution, i=1,…, I and j=1,…,J, x_i is the binary logarithm of the median effective protein concentration level (EC_{50}), a single quantity per dilution series to represent the concentration of the protein, x_i+lj is the binary logarithm of the protein concentration after jth dilution where $l_j = \frac{(1+J)}{2} - j$, ε_{ij} is the error term assumed to have a normal distribution with mean 0 and variance σ_1^2, and $\boldsymbol{\beta}$=$\{\beta_1,\beta_2,\beta_3\}$. Since $\beta_1 = \lim_{x_i \to -\infty} E(y_{ij})$ and $\beta_1 + \beta_2 = \lim_{x_i \to -\infty} E(y_{ij})$, β_1 is interpreted as the lowest intensity level without noise, and β_2 is the increment from the lowest to the highest intensity or the saturation level.

To estimate the relative protein concentration in RPPA, one algorithm based on logistic model fitting used by Hu [12] is given as follows:

The initial intensity data are first transformed as

$$y_{linear_{ij}} = \text{logit}_2 \frac{y_{ij} - \min(Y)}{range(Y)} \quad (2)$$

and initial $\boldsymbol{\beta}$ are set as

$\hat{\beta}_1^{(0)} = \min(Y), \hat{\beta}_2^{(0)} = \max(Y) - \min(Y), \hat{\beta}_3^{(0)} = \hat{\beta}_2^{(0)} / (J-1), Y = \{y_{ij} | i = 1,...,I \text{ and } j = 1,...,J\}$, $range(Y)$=max(Y)−min (Y).

The initial median effective protein concentration level x_i are estimated by using:

$$x_i = median \frac{(y_{linear_i})}{\hat{\beta}_3} + l_j \quad (3)$$

where y_{linear_i} is the mean value among $\{y_{linear_i}\}$

To update the parameters $(\hat{\beta}_1^{(0)}, \hat{\beta}_2^{(0)}, \hat{\beta}_3^{(0)})$ in the nonlinear model, the nonlinear least-squares estimates of $(\hat{\beta}_1^{(1)}, \hat{\beta}_2^{(1)}, \hat{\beta}_3^{(1)})$ were calculated based on the following model [14]:

$$y_{ij} = g(x_i, l_j, \beta) = \beta_1 + \frac{\beta_2}{1+2^{-\beta_3(x_i-l_j)}} + \varepsilon_{ij} \quad (4)$$

After obtaining $\hat{\beta}_1^{(1)}, \hat{\beta}_2^{(1)}, \hat{\beta}_3^{(1)}$, the nonlinear least-square method is used again to update the relative protein level $\boldsymbol{X}$=$\{x_i, i$=1…$I\}$ and σ_1^2. This iteration continues until convergence.

A naïve model for correlating miRNA and protein expression

Since $\boldsymbol{X}$=$\{x_i, i$=1,2,…$I\}$, the log2 transformation of the median effective protein concentration levels, can be estimated from the RPPA, a straightforward way to examine the relationship between miRNA and protein expression levels is through Pearson's correlation coefficients or simple linear regression models, which is referred as the naïve model in this article.

The linear relationship between protein and miRNA in the naïve model can be expressed as: $x_i = f(Z_i) = \alpha_1 + \alpha_2 Z_i + \eta_i$, where $\eta_i \sim N(0, \sigma_0^2)$ and $\{z_i, i$=1,2…$I\}$ are log-transformed expression levels of a specific miRNA from sample i=1,2…I.

The parameter estimates $\hat{\alpha}_1, \hat{\alpha}_2, \hat{\alpha}_0$ can be calculated by using linear regression. $\hat{\alpha}_2$ is our parameter of interest, describing the correlation between a miRNA and protein pair. We can test H_0:α_2=0 to determine if a particular pair of miRNA and protein is related or not.

A hierarchical model for correlating miRNA and protein expression

Although the naïve method is straightforward, uncertainty associated with protein concentration estimates is ignored. As demonstrated in later sections, it leads to less accurate results and significant power loss. Here we propose a nonlinear hierarchical model for studying the relationship between miRNA and protein expression, in which the correlation analysis is integrated with the estimation of protein concentration. The model is given as follows:

$$y_{ij} = g(x_i, l_j, \beta) = \beta_1 + \frac{\beta_2}{1+2^{-\beta_3(x_i-l_j)}} + \varepsilon_{ij} \quad (5)$$

$$x_i = f(Z_i) + \eta_i,$$

$$\eta_i \sim N(0, \sigma_0^2),\ \varepsilon_{ij} \sim N(0, \sigma_0^2),\ \eta_i \perp \varepsilon_{ij} \quad (6)$$

Here (.) is a general function to describe how x_i, the protein level, and z_i, the miRNA expression level, is related. $\boldsymbol{\beta}$= $\{\beta_1,_2,\beta_3\}$ is the parameter vector of the response curve function g(.). To directly

compare with the naïve model, we assume (zi) to be linear in equation (6), that is, $f(Z_i)=\alpha_1+\alpha_2 Z_i$. We further assume that the two error terms, η_i and ε_{ij} are independent of each other. In this hierarchical framework, the relationship between miRNA and protein expression level can be estimated without explicitly quantifying the protein concentration based on intensity data first. This model is referred as the integrated model hereinafter.

The likelihood function for $\boldsymbol{Y}$ and $\boldsymbol{Z}$ can be written as a joint probability function

$$L(\phi,\sigma_0,\sigma_1|Y,Z)=\prod_{\substack{i=1,2,\ldots I\\ j=1,2,\ldots J}}\int_{-\infty}^{+\infty} f_{\varepsilon_{ij}}(y_{ij}|Z_i,\phi,\eta_i,\sigma_1)q_{\eta_i}(\eta_i|\sigma_0)d\eta_i \quad (7)$$

where $\boldsymbol{\phi}=\{\alpha_1,\alpha_2,\beta_1,\beta_2,\beta_3\}$ is a vector including parameters in function $f(.)$ and $g(.)$, $\boldsymbol{Y}=\{y_{ij}|\ i=1,2\ldots I, j=1,2\ldots J\}$ representing the RPPA intensity levels and $\boldsymbol{Z}=\{z_i|i=1,2\ldots I\}$ representing the log-transformed miRNA expression levels.

Computational algorithm

The unknown parameters $\boldsymbol{\phi}=\{\alpha_1,\alpha_2,\beta_1,\beta_2,\beta_3\}$ can be estimated within the maximum likelihood framework. The adaptive Gaussian quadrature method is used to approximate the integral and the dual quasi-Newton method can be further applied in maximizing the likelihood function [15-17]. Our computational algorithm is illustrated in Figure 1. This algorithm is implemented in SAS nlmixed procedure and a SAS macro is available upon request to fit the integrated model.

Based on the idea of Hermite integration for function (x)

$$\int_{-\infty}^{+\infty} f(x)dx=\sum_{k=1}^{m} w_k e^{x_k^2} f(x_k) \quad (8)$$

Our likelihood function can be written as

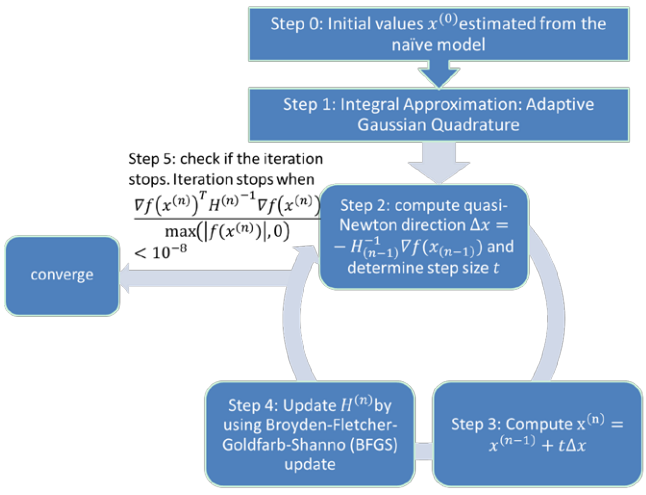

Figure 1: Flow chart of computational algorithm to fit the integrated model based on adaptive Gaussian quadrature method and dual quasi-Newton algorithm. Step 0: estimate the initial value of $\boldsymbol{\phi}_{,0},\sigma_1$, denoted as $x(0)$, by using the naïve model; Step 1: generate the approximate likelihood function by using adaptive Gaussian Quadrature method; Step 2: compute the quasi-Newton direction Δx, determine the step size t to satisfy the Goldstein conditions; Step 3: update parameters x value; Step 4: update Hessian matrix; Step 5: check if the iteration stops. If not, go to Step 2, if yes, the iteration stops. A grid searching with center from the estimates of naïve model was applied in our algorithm.

$$L(\phi,\sigma_0,\sigma_1|Y,Z)=\prod_{\substack{i=1,2,\ldots I\\ j=1,2,\ldots J}}\int_{-\infty}^{+\infty} f_{\varepsilon_{ij}}(y_{ij}|Z_i,\phi,\eta_i,\sigma_1)q_{\eta_i}(\eta_i|\sigma_0)d\eta_i$$

$$\approx\prod_{\substack{i=1,2,\ldots I\\ j=1,2,\ldots J}}\sqrt{2}|\Gamma_i|^{\frac{1}{2}}\sum_{k=1}^{m} f_{\varepsilon_{ij}}(y_{ij}|Z_i,\phi,\sqrt{2}|\Gamma_i|^{\frac{1}{2}}x_k+\hat{\eta}_i,\sigma_1)q_{\eta_i}(\sqrt{2}|\Gamma_i|^{\frac{1}{2}}x_k+\hat{\eta}_i|\sigma_0)w_k e^{x_k^2} \quad (9)$$

m is the number of quadrature points which is set to 5 in our analysis. x_k and w_k denote the standard Gauss-Hermite abscissas and weights; $\hat{\eta}i$ minimizes

$$-\log\left(f_{\varepsilon_{ij}}(y_{ij}|Z_i,\phi,\eta_i,\sigma_1)q_{\eta_i}(\eta_i|\sigma_0)\right) \quad (10)$$

and Γ_i is the Hessian matrix from the minimization.

With the approximate likelihood function, we employed the quasi-Newton algorithm for parameter estimation. Unlike the Newton algorithm, approximate Hessian matrix was used instead of true Hessian matrix in the quasi-Newton algorithm. The step size t was calculated by quadratic interpolation and cubic extrapolation and BFGS method was used to update the approximate Hessian matrix. A grid searching with center from the estimates of Naïve model was applied in our algorithm.

Hypothesis testing

Since it is expected that miRNA negatively regulate the protein level of its target gene, to test if there is a significant relationship between a specific pair of miRNA and protein, the hypothesis test can set up as a one-sided test:

H_0: $\alpha_2=0$ *vs* H_a: $\alpha_2<0$

Once the maximum likelihood estimates are obtained, a likelihood ratio test (LRT), a Wald test or a Score test can be constructed. However, LRT can be very time consuming and is not appropriate for one–sided test. For Score test, the confidence interval of α_2 is difficult to be calculated. Thus Wald tests were used in our simulation and real data example, and its test statistic is:

$T.S.=\dfrac{\hat{\alpha}_2}{I(\hat{\phi})^{\frac{1}{2}}_{\alpha_2}}\sim N(0,1)$ *under* H_0, where $(\boldsymbol{\phi})$ represent the fisher information matrix of the likelihood function. The null hypothesis was rejected when p-value was above 0.05 in our simulation study.

Simulation studies

Extensive simulation studies were carried out to examine the performance of our proposed integrated model and to compare with the naïve model approach. Protein intensities were generated by using a sigmoidal response curve (Figure 2a). And a typical miRNA expression distribution in the TCGA data was borrowed in this simulation to mimic the real data and generate protein EC_{50S} (Figure 2b). Also, the true values of $\{\beta_1,\beta_2,\beta_3,\sigma_0,\sigma_1\}$ were set as {50, 30000, 1, 1, and 300} to mimic parameter values estimated from a real TCGA ovarian cancer data set. Different strengths of correlation between miRNA and protein expression levels, as characterized by α_2, were examined in a range from 0, which represents the null hypothesis, to -1.5, which yields the power of 1 for the integrated method. In order to investigate the performance of two models with protein intensity values located in different areas of the sigmoidal curve, α_1 was set as 0 and 5 corresponding to the middle part and upper part of sigmoidal curve, respectively. The upper part of a sigmoidal curve corresponds to a scenario where most of intensity levels are close to the saturation point. The RPPA intensity levels range between 10 and 30100. An illustration of the sigmoidal curve used to generate simulated data was showed in Figure 2a. The locations of

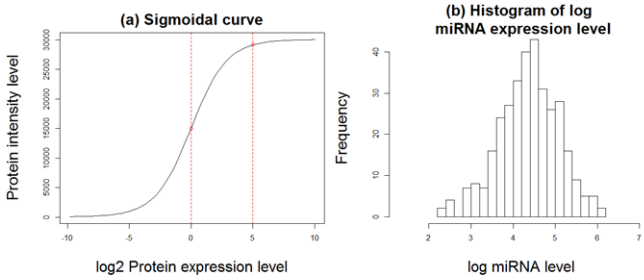

Figure 2: An illustration of (a) a sigmoidal shape response curve. When α_1 was set to be 0, the center of the EC50s would located at 0; When α_1 was set to be 5, the center of EC50s would located at 5; (b) distribution of a typical miRNA expression in the TCGA data we used in the simulation.

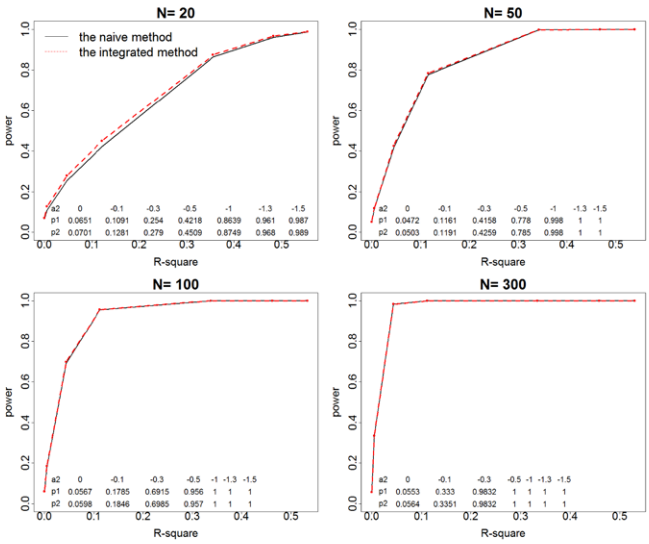

Figure 3: Power curve of the naïve model (solid line) and the integrated model (dashed line) according to different simulation scenarios: sample size ranged from 20 to 300 and the protein intensities were located in the middle part of a sigmoidal curve. Detection powers (type I error if α_2=0) denoted by p_1 and p_2 under different correlation strengths were report on the bottom of each plot for the naïve and integrated models, respectively. Both models can well control the pre-specified type-I error when sample size were bigger than 50. Two models had similar detection performance, especially when sample size increased.

protein intensity center were marked by circles. If simulated intensity values are beyond the imaging boundary, they would be replaced with the boundary value with small error (Gaussian distributed with mean 0 and standard deviation 5). 1000 simulations were carried out for each parameter setting under different sample sizes (N=20, 50, 100 and 300). Generally, there are 5 diluted samples in one dilution series, so J=5 were used in our simulation setting. Pre-specified Type I error was set to be 0.05.

The false positive rates and detection powers for miRNA targets for both the integrated model and the naïve model under different sample sizes were shown in Figures 3 and 4. It is clear that when there was no relationship between miRNA and protein (α_2=0), both models can well control the pre-specified type-I error when sample size were bigger than 50. The integrated model was consistently more powerful than the naïve model, especially when the RPPA intensity levels are

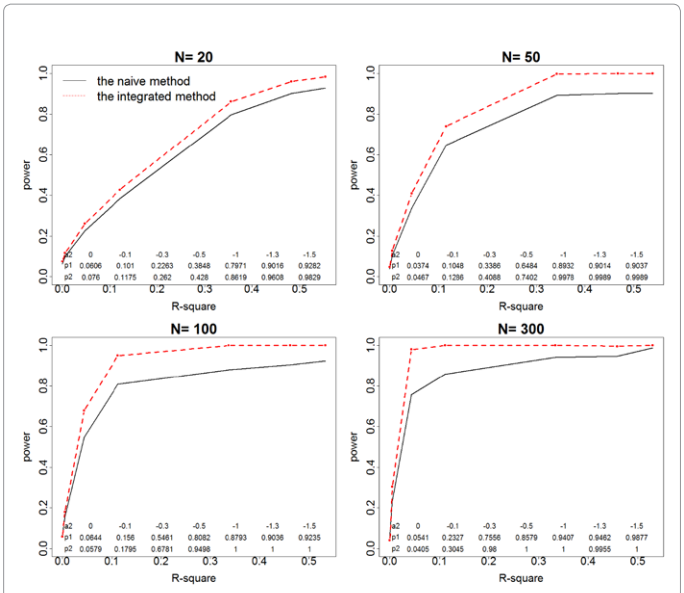

Figure 4: Power curves of the naïve model (solid line) and the integrated model (dashed line) according different simulation scenarios: sample size ranged from 20 to 300 and the protein intensities were located in the upper part of a sigmoidal curve. Detection powers (type I error if α_2=0) denoted by p_1 and p_2 under different correlation strength were report on the bottom of each figure for the naïve and integrated models, respectively. Both models can well control the pre-specified type-I error when sample size were bigger than 50. The integrated model was consistently more powerful than the naïve model.

close to the boundaries of imaging limits (Figure 4). Table A1-A2 in appendix listed the detailed point estimates of all parameters and their corresponding standard errors. Figure A1 and A2 in appendix illustrated the variations of the point estimates of α_2 under different simulation settings. The integrated model consistently yielded parameter estimates of α_2 with similar or much less standard errors than those from the naïve model. When the RPPA intensities reached the upper flatter part of the sigmoidal curve, which caused information loss because of intensity level truncation at the saturation points, both the naïve and the integrated method over-estimated β_1, which represents the lower imaging limits. However, in this situation the integrated method still had a much larger detection power than the naïve method (Figure 4).

Analysis of TCGA Ovarian Cancer Data

Both models were applied onto an ovarian cancer dataset from the TCGA project. In this dataset, there were 333 ovarian cancer samples with both miRNA and RPPA data available. 352 miRNAs having more than 50% of non-zero counts and 165 proteins were included in our analyses.

The results from both naïve and integrated models on predicting miRNA targets were reported in Table 1. False Discover Rate (FDR) at 10% was used to adjust for multiple testing [18]. The integrated model approach we proposed found 1106 potential miRNA-protein pairs, 797 of which were on non-phosphorylated protein array. 822 pairs were found on non-phosphorylated protein array: 250 out of them were found by integrated model only and 25 pairs were found by naïve model only. Integrated model found significantly more number of potential miRNA-protein pairs (P<0.0001 according to McNemar's test). Furthermore, we compared our results with miRNA targets identified by miRanda algorithm [19-22]. 98 targets, which were found by both the integrated and the naïve model, and 31 targets, which

Table 1: Table for the detailed point estimates of all unknown parameters and their standard error;Sample size was from 20 to 300 and the protein intensity located in the middle part of sigmoidal curve; the integrated model had a similar performance as the naïve model.

	α_1	α_2	β_1	β_2	β_3	σ_0	σ_1
Sample size	20						
true value	0	0	50	30000	1	1	500
naive model	0.0213 (0.0517)	-0.0063 (0.0117)	78.13 (22.56)	29958.77 (31.48)	1.0022 (0.0014)	0.9809 (0.0053)	463.61 (1.34)
integrated model	0.015 (0.052)	-0.0062 (0.0117)	142.07 (15.3)	29881.73 (28.8)	1.0077 (0.0014)	0.9298 (0.0051)	490.89 (1.24)
true value	0	-0.1	50	30000	1	1	500
naive model	-0.0062 (0.0057)	-0.1066 (0.0117)	78.43 (22.69)	29954.12 (31.17)	1.0023 (0.0014)	0.981 (0.0053)	463.75 (1.34)
integrated model	-0.0106 (0.0068)	-0.1067 (0.0117)	136.82 (15.25)	29875.35 (28.62)	1.0078 (0.0014)	0.9299 (0.005)	490.51 (1.23)
true value	0	-0.3	50	30000	1	1	500
naive model	-0.0015 (0.0057)	-0.3067 (0.0117)	83.04 (23.4)	29904.9 (31.25)	1.0044 (0.0014)	0.9811 (0.0053)	464.85 (1.38)
integrated model	-0.0126 (0.0068)	-0.3071 (0.0117)	168.89 (15.35)	29827.69 (29.14)	1.0102 (0.0014)	0.93 (0.0051)	491.49 (1.23)
true value	0	-0.5	50	30000	1	1	500
naive model	-0.0015 (0.0057)	-0.5063 (0.0117)	81.23 (22.74)	29909.99 (30.21)	1.0045 (0.0014)	0.9807 (0.0053)	464.58 (1.36)
integrated model	-0.0119 (0.0068)	-0.5069 (0.0117)	161.52 (14.84)	29838.19 (28.02)	1.0096 (0.0014)	0.9297 (0.0051)	491.18 (1.23)
true value	0	-1	50	30000	1	1	500
naive model	-0.0043 (0.0061)	-1.0021 (0.0117)	23.03 (20.93)	30048.43 (26.41)	0.9997 (0.0012)	0.9795 (0.0053)	465.42 (1.4)
integrated model	-0.0105 (0.0068)	-1.005 (0.0117)	91.21 (13.22)	29964.21 (24.28)	1.003 (0.0012)	0.9298 (0.0051)	491.06 (1.27)
true value	0	-1.3	50	30000	1	1	500
naive model	-0.0055 (0.006)	-1.3033 (0.0117)	39.67 (18.69)	30027.79 (24.25)	1.0018 (0.0012)	0.9792 (0.0053)	465.7 (1.37)
integrated model	-0.0099 (0.0067)	-1.3077 (0.0118)	96.34 (11.97)	29952.63 (22.46)	1.0035 (0.0011)	0.9301 (0.005)	491.25 (1.25)
true value	0	-1.5	50	30000	1	1	500
naive model	-0.0096 (0.0063)	-1.5032 (0.0117)	83.81 (17.38)	29973.69 (22.32)	1.0042 (0.0011)	0.9789 (0.0053)	464.47 (1.35)
integrated model	-0.0111 (0.0069)	-1.5086 (0.0117)	124.24 (11.18)	29909.02 (20.75)	1.0054 (0.0011)	0.93 (0.0051)	491.11 (1.28)
Sample size	50						
true value	0	0	50	30000	1	1	500
naive model	-0.023 (0.0283)	0.0054 (0.0064)	-11.3 (16.58)	30137.24 (20.17)	0.9952 (9e-04)	0.9923 (0.0032)	457.55 (0.85)
integrated model	-0.0259 (0.0284)	0.0053 (0.0064)	43.36 (9.77)	30057.24 (18.46)	0.9982 (9e-04)	0.9719 (0.0032)	495.97 (0.79)
true value	0	-0.1	50	30000	1	1	500
naive model	-0.0012 (0.0041)	-0.0946 (0.0064)	-6.46 (16.12)	30141.23 (19.69)	0.9951 (9e-04)	0.9925 (0.0032)	457.14 (0.84)
integrated model	-0.0026 (0.0043)	-0.0947 (0.0064)	39.43 (9.46)	30061.21 (18.05)	0.9982 (8e-04)	0.972 (0.0032)	495.79 (0.79)
true value	0	-0.3	50	30000	1	1	500
naive model	0.0021 (0.0041)	-0.2942 (0.0064)	-14.38 (15.88)	30131.06 (18.59)	0.9954 (8e-04)	0.9923 (0.0032)	458.04 (0.86)
integrated model	-9e-04 (0.0044)	-0.2945 (0.0064)	36.9 (8.99)	30053.19 (17.01)	0.9983 (8e-04)	0.9719 (0.0032)	496.54 (0.78)
true value	0	-0.5	50	30000	1	1	500
naive model	0.0031 (0.004)	-0.4939 (0.0064)	-10.89 (15.49)	30113.24 (17.77)	0.9965 (8e-04)	0.9919 (0.0032)	457 (0.84)
integrated model	-0.002 (0.0044)	-0.4946 (0.0064)	46.42 (8.56)	30042.02 (16.43)	0.9988 (8e-04)	0.9716 (0.0032)	496.05 (0.79)
true value	0	-1	50	30000	1	1	500
naive model	-0.0031 (0.0042)	-0.9927 (0.0064)	16.45 (13.86)	30112.04 (16.06)	0.998 (8e-04)	0.9915 (0.0032)	457.22 (0.82)
integrated model	-0.0022 (0.0044)	-0.9948 (0.0064)	46.61 (7.86)	30043.54 (14.75)	0.9986 (7e-04)	0.9719 (0.0032)	496.19 (0.79)
true value	0	-1.3	50	30000	1	1	500
naive model	-0.0068 (0.0043)	-1.2911 (0.0064)	48.01 (13.45)	30080.17 (14.29)	1.0002 (7e-04)	0.9911 (0.0032)	457.21 (0.82)
integrated model	-0.0018 (0.0044)	-1.2949 (0.0064)	60.83 (7.18)	30013.75 (13.47)	0.9997 (7e-04)	0.9721 (0.0032)	496.15 (0.79)
true value	0	-1.5	50	30000	1	1	500
naive model	-0.0078 (0.0041)	-1.4898 (0.0064)	77.09 (11.46)	30027.67 (13.43)	1.0032 (7e-04)	0.9909 (0.0032)	456.69 (0.78)
integrated model	-0.0026 (0.0043)	-1.4944 (0.0064)	82.21 (6.6)	29975.26 (12.74)	1.0017 (7e-04)	0.972 (0.0032)	496.5 (0.77)
Sample size	100						
true value	0	0	50	30000	1	1	500
naive model	0.0124 (0.0207)	-0.0032 (0.0047)	-21.78 (12.82)	30189.17 (14.32)	0.9927 (6e-04)	0.997 (0.0022)	455.17 (0.62)
integrated model	0.0143 (0.0208)	-0.0033 (0.0047)	7.17 (6.74)	30116.73 (12.96)	0.9951 (6e-04)	0.9863 (0.0022)	498.45 (0.57)
true value	0	-0.1	50	30000	1	1	500
naive model	0.0029 (0.0032)	-0.1028 (0.0047)	-46.45 (12.49)	30192.3 (13.75)	0.9929 (6e-04)	0.9965 (0.0022)	454.27 (0.6)
integrated model	-5e-04 (0.0032)	-0.1029 (0.0047)	1.55 (6.47)	30125.41 (12.4)	0.9948 (6e-04)	0.9859 (0.0022)	498.08 (0.56)
true value	0	-0.3	50	30000	1	1	500
naive model	3e-04 (0.0033)	-0.3033 (0.0047)	-26.94 (12.46)	30177.98 (13.77)	0.9932 (6e-04)	0.9968 (0.0022)	455.26 (0.6)
integrated model	-9e-04 (0.0032)	-0.3036 (0.0047)	11.3 (6.47)	30110.92 (12.44)	0.9951 (6e-04)	0.9861 (0.0022)	498.77 (0.56)
true value	0	-0.5	50	30000	1	1	500
naive model	0.0034 (0.0033)	-0.5024 (0.0047)	-29.46 (12.41)	30152.94 (12.87)	0.9948 (6e-04)	0.9968 (0.0022)	454.68 (0.59)

integrated model	-0.002 (0.0032)	-0.5029 (0.0047)	23.79 (6.41)	30091.34 (11.81)	0.996 (6e-04)	0.9863 (0.0022)	498.68 (0.56)
true value	0	-1	50	30000	1	1	500
naive model	-0.0063 (0.0033)	-1.0002 (0.0047)	18.58 (10.56)	30140.4 (11.11)	0.9961 (5e-04)	0.9965 (0.0022)	454.05 (0.58)
integrated model	-0.0024 (0.0032)	-1.0018 (0.0047)	31.28 (5.38)	30081.86 (10.35)	0.9964 (5e-04)	0.9864 (0.0022)	498.21 (0.57)
true value	0	-1.3	50	30000	1	1	500
naive model	-0.0072 (0.0033)	-1.3008 (0.0047)	47.51 (9.63)	30088.26 (9.9)	0.9992 (5e-04)	0.9967 (0.0022)	453.78 (0.59)
integrated model	-0.0024 (0.0032)	-1.3036 (0.0047)	52.33 (4.87)	30038.92 (9.46)	0.9982 (5e-04)	0.9871 (0.0022)	498.32 (0.59)
true value	0	-1.5	50	30000	1	1	500
naive model	-0.0066 (0.0032)	-1.5001 (0.0047)	65.64 (8.32)	30046.58 (8.83)	1.0018 (4e-04)	0.996 (0.0022)	452.58 (0.56)
integrated model	-8e-04 (0.0032)	-1.5037 (0.0047)	62.17 (4.51)	30006.08 (8.55)	0.9998 (4e-04)	0.9864 (0.0022)	498.25 (0.58)
Sample size	300						
true value	0	0	50	30000	1	1	500
naive model	-0.0029 (0.0118)	-7e-04 (0.0027)	-7.69 (8.36)	30141.18 (8.44)	0.9945 (4e-04)	0.9998 (0.0014)	451.18 (0.34)
integrated model	-0.0039 (0.0118)	-7e-04 (0.0027)	17.74 (3.87)	30099.42 (7.63)	0.9956 (4e-04)	0.9953 (0.0014)	499.45 (0.32)
true value	0	-0.1	50	30000	1	1	500
naive model	3e-04 (0.0023)	-0.1009 (0.0026)	-45.21 (8.74)	30156.77 (7.84)	0.9938 (4e-04)	0.9999 (0.0014)	451.88 (0.34)
integrated model	-0.0084 (0.002)	-0.1009 (0.0026)	11.41 (3.65)	30117.72 (7.15)	0.9947 (3e-04)	0.9955 (0.0014)	500 (0.32)
true value	0	-0.3	50	30000	1	1	500
naive model	-0.0038 (0.0024)	-0.3005 (0.0027)	-19.8 (8.81)	30144.6 (8.1)	0.9945 (4e-04)	0.9996 (0.0014)	451.86 (0.35)
integrated model	-0.0069 (0.0019)	-0.3006 (0.0027)	14.95 (3.71)	30101.39 (7.38)	0.9955 (4e-04)	0.9953 (0.0014)	499.85 (0.31)
true value	0	-0.5	50	30000	1	1	500
naive model	-0.0041 (0.0023)	-0.5006 (0.0026)	-16.25 (8.32)	30142.07 (7.35)	0.9948 (3e-04)	0.9996 (0.0014)	451.4 (0.33)
integrated model	-0.0085 (0.0019)	-0.5009 (0.0026)	22.01 (3.48)	30102.75 (6.82)	0.9954 (3e-04)	0.9953 (0.0014)	499.8 (0.32)
true value	0	-1	50	30000	1	1	500
naive model	-0.0121 (0.0023)	-0.999 (0.0027)	30.28 (7.06)	30107.97 (6.46)	0.9968 (3e-04)	0.9996 (0.0014)	451 (0.33)
integrated model	-0.0082 (0.002)	-0.9999 (0.0027)	32.49 (3.08)	30070.72 (6.22)	0.9967 (3e-04)	0.9955 (0.0014)	499.92 (0.33)
true value	0	-1.3	50	30000	1	1	500
naive model	-0.0101 (0.0021)	-1.2999 (0.0028)	47.45 (5.33)	30058.55 (5.39)	0.9997 (3e-04)	1.0019 (0.0027)	448.96 (0.31)
integrated model	-0.0077 (0.002)	-1.3008 (0.0028)	49.28 (2.79)	30036.58 (5.22)	0.9983 (3e-04)	0.9955 (0.0014)	499.31 (0.34)
true value	0	-1.5	50	30000	1	1	500
naive model	-0.0106 (0.0021)	-1.4962 (0.0027)	47.23 (4.56)	30059.42 (5.23)	1.0004 (3e-04)	0.9997 (0.0015)	450.03 (1.52)
integrated model	-0.0091 (0.0021)	-1.4986 (0.0028)	49.02 (2.61)	30043.6 (5.15)	0.9979 (3e-04)	0.9955 (0.0014)	499.52 (0.35)

Table 2: Table for the detailed point estimates of all unknown parameters and their standard error;Sample size was from 20 to 300and the protein intensity located in the upper part of sigmoidal curve. Truncation was applied to the boundary of intensity level; the integrated model consistently yielded parameter estimates of α_2 with similar or much less standard errors than the naïve model.

	α_1	α_2	β_1	β_2	β_3	σ_0	σ_1
Sample size	20						
true value	5	0	50	30000	1	1	500
naive model	2.3538 (0.0337)	0.0108 (0.0348)	21673.99 (73.67)	8063.19 (72.22)	1.8432 (0.0062)	1.5515 (0.1377)	505.9 (4.52)
integrated model	4.4653 (0.08)	-0.0161 (0.0139)	-274276.76 (52197.04)	304133.74 (52200.42)	1.2805 (0.011)	0.9099 (0.0111)	457.39 (1.95)
true value	5	-0.1	50	30000	1	1	500
naive model	2.3656 (0.0399)	-0.0895 (0.0592)	21700.84 (71.7)	8041.22 (70.25)	1.8401 (0.0059)	1.6134 (0.1588)	504.84 (3.24)
integrated model	4.5686 (0.0859)	-0.0693 (0.0418)	-330800.61 (56594.51)	360639.78 (56591.54)	1.2918 (0.0288)	0.9732 (0.0742)	458.96 (2)
true value	5	-0.3	50	30000	1	1	500
naive model	2.3695 (0.0275)	-0.3577 (0.0482)	21516.03 (74.6)	8221.13 (73.15)	1.8385 (0.0057)	1.5135 (0.1068)	505.61 (3.97)
integrated model	4.403 (0.0769)	-0.308 (0.0123)	-249677.33 (50408.57)	279512.95 (50405.41)	1.2762 (0.0105)	0.8937 (0.0099)	456.25 (1.72)
true value	5	-0.5	50	30000	1	1	500
naive model	2.4446 (0.0374)	-0.7107 (0.0782)	21269.05 (74.86)	8464.35 (73.51)	1.8481 (0.0059)	1.6564 (0.1521)	507.56 (2.77)
integrated model	4.5227 (0.0783)	-0.5035 (0.0123)	-250395.86 (48590.31)	280258.79 (48592.42)	1.2486 (0.0097)	0.8891 (0.0102)	457.35 (1.82)
true value	5	-1	50	30000	1	1	500
naive model	2.7712 (0.0505)	-1.4615 (0.1208)	19902.57 (90.02)	9814.9 (88.76)	1.8388 (0.0058)	2.1685 (0.1959)	527.34 (4.87)
integrated model	4.1187 (0.0636)	-1.0024 (0.0148)	-52274.05 (21283.7)	82100.65 (21281.33)	1.2984 (0.0263)	0.8417 (0.0365)	469.74 (2.81)
true value	5	-1.3	50	30000	1	1	500
naive model	2.9411 (0.0548)	-1.7328 (0.0838)	18770.02 (98.58)	10936.33 (97.49)	1.828 (0.0054)	2.2838 (0.2277)	539.5 (4.31)
integrated model	4.1799 (0.0528)	-1.3159 (0.0145)	-81574.65 (30566.75)	111394.19 (30567.8)	1.2845 (0.0095)	0.8634 (0.0125)	478.65 (2.39)
true value	5	-1.5	50	30000	1	1	500
naive model	3.2206 (0.0717)	-2.3778 (0.1593)	18002.82 (105.51)	11696.6 (104.59)	1.8231 (0.0057)	2.9557 (0.2621)	560.41 (7.25)
integrated model	3.6493 (0.6203)	-0.964 (0.6069)	-51974.4 (22391.12)	81776.04 (22386.56)	1.2932 (0.0201)	0.8548 (0.0355)	488.64 (3.71)
Sample size	50						
true value	5	0	50	30000	1	1	500

naive model	2.7437 (0.0369)	-0.0469 (0.0526)	20499.39 (63.98)	9225.41 (62.87)	1.7402 (0.0037)	2.7635 (0.2377)	485.25 (2.14)
integrated model	3.5198 (0.0405)	0.0089 (0.0067)	8598.57 (1581.12)	21172.62 (1582.55)	1.4285 (0.0103)	0.8595 (0.0138)	489.77 (1.59)
true value	5	-0.1	50	30000	1	1	500
naive model	2.7316 (0.0347)	-0.1643 (0.0384)	20463.66 (65.62)	9261.85 (64.57)	1.738 (0.0038)	2.6338 (0.2266)	484.29 (1.72)
integrated model	3.4811 (0.0385)	-0.0898 (0.0067)	9927.86 (1621.29)	19842.78 (1622.67)	1.434 (0.0104)	0.8728 (0.0129)	491.19 (1.61)
true value	5	-0.3	50	30000	1	1	500
naive model	2.8069 (0.0401)	-0.4472 (0.047)	20293.49 (66.02)	9426.7 (65.05)	1.7416 (0.0037)	2.9565 (0.2576)	486.58 (1.97)
integrated model	3.4894 (0.0357)	-0.2882 (0.0067)	12135.89 (534.51)	17635.35 (537.21)	1.4246 (0.0101)	0.8701 (0.0131)	491.18 (1.66)
true value	5	-0.5	50	30000	1	1	500
naive model	2.828 (0.0387)	-0.6441 (0.0451)	19946.91 (69.44)	9770.55 (68.46)	1.7402 (0.0038)	2.8163 (0.2509)	491.23 (2.77)
integrated model	3.5327 (0.0365)	-0.4769 (0.0067)	11365.82 (735.99)	18404.38 (738.2)	1.4188 (0.01)	0.8762 (0.0124)	493.4 (1.7)
true value	5	-1	50	30000	1	1	500
naive model	3.2183 (0.047)	-1.7113 (0.0905)	18367.63 (79.4)	11331.51 (78.56)	1.7405 (0.0037)	3.9333 (0.301)	506.65 (2.69)
integrated model	3.4259 (0.029)	-0.9716 (0.0072)	13477.54 (288.17)	16260.6 (291.47)	1.4497 (0.0086)	0.7908 (0.0171)	512.56 (1.84)
true value	5	-1.3	50	30000	1	1	500
naive model	3.5889 (0.0593)	-2.5651 (0.1361)	17174.96 (86.16)	12514.49 (85.49)	1.7375 (0.0037)	5.4373 (0.3774)	521.52 (3.13)
integrated model	3.2866 (0.1729)	-1.4043 (0.1428)	13337.94 (260.58)	16383.67 (263.67)	1.4403 (0.0146)	0.8708 (0.1229)	528.37 (2.55)
true value	5	-1.5	50	30000	1	1	500
naive model	3.8296 (0.0621)	-2.9831 (0.1416)	16141.61 (89.86)	13546.24 (89.49)	1.7198 (0.0039)	6.1208 (0.3784)	523.94 (2.07)
integrated model	3.305 (0.1669)	-1.3648 (0.105)	13436.45 (198.21)	16273.32 (201.3)	1.4225 (0.0332)	0.9029 (0.1719)	536.53 (2.56)
Sample size	100						
true value	5	0	50	30000	1	1	500
naive model	2.9087 (0.0269)	-0.039 (0.0434)	19661.6 (56.83)	10058.46 (56.2)	1.6748 (0.003)	3.337 (0.2366)	468.53 (1.22)
integrated model	3.0493 (0.0261)	-0.0055 (0.006)	16387.53 (641.05)	13333.07 (642.19)	1.5292 (0.0075)	0.8232 (0.0178)	501.83 (1.1)
true value	5	-0.1	50	30000	1	1	500
naive model	2.9097 (0.0291)	-0.1508 (0.043)	19584.67 (57.9)	10137.22 (57.29)	1.6675 (0.0028)	3.2625 (0.2545)	469.76 (1.53)
integrated model	3.0247 (0.0234)	-0.0985 (0.0065)	17062.36 (191.54)	12657.31 (194.2)	1.5329 (0.0073)	0.8748 (0.0133)	502.86 (1.06)
true value	5	-0.3	50	30000	1	1	500
naive model	2.9106 (0.0275)	-0.3621 (0.0361)	19313.04 (62.78)	10404.89 (62.09)	1.6712 (0.003)	3.0649 (0.2302)	469.78 (0.91)
integrated model	3.0442 (0.0224)	-0.3021 (0.0073)	16981.12 (176.62)	12738.09 (179.23)	1.5236 (0.007)	0.8185 (0.0172)	504.55 (1.09)
true value	5	-0.5	50	30000	1	1	500
naive model	3.0186 (0.0323)	-0.7679 (0.044)	18919.14 (64.29)	10793.17 (63.66)	1.674 (0.003)	3.701 (0.2824)	474.8 (1.61)
integrated model	3.0784 (0.0226)	-0.4853 (0.0049)	16620.4 (198.41)	13095.57 (200.87)	1.5193 (0.0068)	0.8203 (0.0165)	508.61 (1.12)
true value	5	-1	50	30000	1	1	500
naive model	3.5281 (0.0442)	-2.0565 (0.0999)	17213.8 (74.03)	12482.15 (73.63)	1.6745 (0.003)	5.9013 (0.3507)	486.43 (0.92)
integrated model	3.1546 (0.0163)	-0.9644 (0.0055)	16182.07 (131.53)	13518.68 (133.43)	1.5056 (0.0053)	0.7447 (0.0202)	521.9 (1.12)
true value	5	-1.3	50	30000	1	1	500
naive model	3.8155 (0.0476)	-2.6141 (0.0999)	15813.29 (80.09)	13875.57 (79.85)	1.6668 (0.0034)	7.1509 (0.3873)	504.16 (2.87)
integrated model	3.28 (0.0142)	-1.2628 (0.0074)	15230.07 (110.54)	14467.41 (111.99)	1.4792 (0.0047)	0.7278 (0.0212)	531.28 (1.16)
true value	5	-1.5	50	30000	1	1	500
naive model	4.23 (0.0626)	-3.6045 (0.1408)	14844.17 (83.8)	14844.17 (83.59)	1.6571 (0.0034)	9.335 (0.4778)	513.6 (2.09)
integrated model	3.4028 (0.016)	-1.4779 (0.0122)	14282.26 (116.92)	15415.65 (118.47)	1.4536 (0.0046)	0.6573 (0.0252)	539.12 (1.27)
Sample size	300						
true value	5	0	50	30000	1	1	500
naive model	3.0135 (0.0208)	0.0285 (0.0232)	18437.53 (67.92)	11288.37 (67.65)	1.5908 (0.003)	3.2476 (0.263)	451.57 (1.21)
integrated model	2.9 (0.0112)	5e-04 (0.0039)	18348.42 (75.58)	11365.95 (76.43)	1.5243 (0.0043)	0.8799 (0.0187)	498.43 (0.68)
true value	5	-0.1	50	30000	1	1	500
naive model	3.0361 (0.0228)	-0.1808 (0.0329)	18456.78 (69.96)	11268.42 (69.74)	1.592 (0.0032)	3.577 (0.2943)	454.1 (2.08)
integrated model	2.9366 (0.0163)	-0.0989 (0.0074)	18113.81 (121.05)	11603.85 (122.77)	1.516 (0.0054)	0.879 (0.0201)	496.92 (0.77)
true value	5	-0.3	50	30000	1	1	500
naive model	3.0804 (0.027)	-0.3768 (0.0336)	18175.54 (74.23)	11545.95 (73.97)	1.5939 (0.0032)	4.1281 (0.3787)	453.35 (1.29)
integrated model	2.9395 (0.0132)	-0.2858 (0.004)	18058.62 (94.19)	11655.43 (95.21)	1.5166 (0.0046)	0.8667 (0.0213)	498.87 (0.69)
true value	5	-0.5	50	30000	1	1	500
naive model	3.1502 (0.0254)	-0.7234 (0.0412)	17717.61 (82.68)	11998.41 (82.46)	1.5974 (0.0034)	3.9477 (0.3312)	454.13 (0.75)
integrated model	2.9937 (0.0129)	-0.4811 (0.0042)	17680.24 (87.96)	12031.57 (88.86)	1.5063 (0.0047)	0.8291 (0.0251)	500.36 (0.78)
true value	5	-1	50	30000	1	1	500
naive model	3.5669 (0.043)	-1.7535 (0.09)	15740.25 (113.86)	13964.36 (113.86)	1.5926 (0.0043)	6.4576 (0.5025)	471.3 (3.33)
integrated model	3.2607 (0.0177)	-0.9702 (0.0074)	15650.42 (130.59)	14066.12 (132.08)	1.4461 (0.0057)	0.8718 (0.0259)	505.15 (0.98)
true value	5	-1.3	50	30000	1	1	500
naive model	4.0045 (0.1514)	-2.2565 (0.5547)	13772.02 (120.38)	15929.25 (120.41)	1.5632 (0.0045)	12.2208 (2.356)	480.58 (3.11)
integrated model	3.1969 (0.3036)	-0.7316 (0.5495)	13720.47 (126.43)	16004.76 (128)	1.3919 (0.0097)	2.9218 (2.2545)	514.38 (4.56)
true value	5	-1.5	50	30000	1	1	500
naive model	4.4603 (0.0723)	-3.707 (0.1756)	12633.68 (117.4)	17067.83 (117.75)	1.5489 (0.0043)	12.0708 (0.7155)	485.18 (1.18)
integrated model	3.6474 (0.0193)	-1.4779 (0.0129)	12443.71 (145.16)	17289.63 (147.48)	1.3512 (0.0055)	0.6374 (0.0466)	510.48 (1.31)

Table 3: A list of miRNA/protein pairs suggested by the naïve model and the integrated model and they were classed into three groups: "Found by the integrated model only", "Found by both the integrated model and the naïve model" and "Found by the naïve model only". Pairs found by the integrated model were sorted by ascending order of adjusted p-values from the integrated model and the naïve model, respectively. Pairs found by the naïve model only were sorted by ascending order of adjusted p-values from the naïve model andintegrated model, respectively.In addition, a number "1" will mark under the column for pairs found by MirTarbase, MirTarBase with strong experimental evidences or miRanda, and those pairs will be list on the top of each group after pairs got ordered.

Composite Element REF	miRNA	Corresponding genes			MirTarbase	MirTarbase (Supported by strong experimental evidences)	miRanda
Found by the integrated model only							
p53-r-v	hsa-mir-605	TP53			1	1	
n-cadherin-r-v	hsa-mir-511-2	CDH2					1
akt-r-v	hsa-mir-511-1	AKT1	AKT2	AKT3			1
eef2k-r-v	hsa-mir-486	EEF2K					1
p53-r-v	hsa-mir-181a-1	TP53					1
smad4-m-c	hsa-mir-142	SMAD4					1
c-met-m-c	hsa-mir-223	MET					1
caspase-8-m-c	hsa-mir-541	CASP8					1
pcna-m-v	hsa-mir-223	PCNA					1
n-cadherin-r-v	hsa-mir-146a	CDH2					1
syk-m-v	hsa-mir-369	SYK					1
alpha-catenin-m-v	hsa-mir-22	CTNNA1					1
smad3-r-v	hsa-mir-142	SMAD3					1
chk1-r-v	hsa-mir-605	CHEK1					1
er-alpha-r-v	hsa-mir-181a-2	ESR1					1
aib1-m-v	hsa-mir-605	NCOA3					1
rad50-m-c	hsa-mir-22	RAD50					1
caspase-8-m-c	hsa-mir-483	CASP8					1
syk-m-v	hsa-mir-193a	SYK					1
jnk2-r-c	hsa-mir-511-1	MAPK9					1
p53-r-v	hsa-mir-588	TP53					1
dj-1-r-c	hsa-mir-145	PARK7					1
akt-r-v	hsa-mir-142	AKT1	AKT2	AKT3			1
p27-r-v	hsa-mir-205	CDKN1B					1
beta-catenin-r-v	hsa-mir-485	CTNNB1					1
c-kit-r-v	hsa-mir-21	KIT					1
chk1-r-v	hsa-let-7b	CHEK1					1
b-raf-m-na	hsa-mir-511-1	BRAF					1
stat5-alpha-r-v	hsa-mir-1224	STAT5A					1
igf-1r-beta-r-c	hsa-let-7b	IGF1R					1
pea-15-r-v	hsa-mir-541	PEA15					1
beta-catenin-r-v	hsa-mir-1228	CTNNB1					1
c-raf-r-v	hsa-mir-1295	RAF1					
msh2-m-c	hsa-mir-1247	MSH2					
msh2-m-c	hsa-mir-199a-1	MSH2					
aib1-m-v	hsa-mir-150	NCOA3					
bcl-2-m-v	hsa-mir-1307	BCL2					
alpha-catenin-m-v	hsa-mir-511-2	CTNNA1					
alpha-catenin-m-v	hsa-mir-511-1	CTNNA1					
aib1-m-v	hsa-mir-214	NCOA3					
bcl-2-m-v	hsa-mir-652	BCL2					
ar-r-v	hsa-mir-224	AR					
k-ras-m-c	hsa-mir-150	KRAS					
ciap-r-v	hsa-mir-223	BIRC2					
ciap-r-v	hsa-mir-140	BIRC2					
ciap-r-v	hsa-mir-511-2	BIRC2					
aib1-m-v	hsa-mir-1228	NCOA3					
claudin-7-r-v	hsa-mir-140	CLDN7					
ar-r-v	hsa-mir-1228	AR					
bcl-xl-r-c	hsa-mir-1295	BCL2L1					
ar-r-v	hsa-mir-511-1	AR					
eef2k-r-v	hsa-mir-181a-2	EEF2K					
tau-m-c	hsa-mir-142	MAPT					
cdk1-r-v	hsa-mir-1247	CDC2					

cdk1-r-v	hsa-let-7a-3	CDC2					
cdk1-r-v	hsa-let-7a-1	CDC2					
cdk1-r-v	hsa-let-7a-2	CDC2					
eef2k-r-v	hsa-mir-1908	EEF2K					
p27-r-v	hsa-mir-136	CDKN1B					
eef2k-r-v	hsa-mir-134	EEF2K					
setd2-r-na	hsa-mir-511-2	SETD2					
smad1-r-v	hsa-mir-483	SMAD1					
irs1-r-v	hsa-mir-511-1	IRS1					
p21-r-c	hsa-mir-150	CDKN1A					
ar-r-v	hsa-mir-1307	AR					
bcl-2-m-v	hsa-mir-1295	BCL2					
n-cadherin-r-v	hsa-mir-142	CDH2					
smad4-m-c	hsa-mir-1295	SMAD4					
cdk1-r-v	hsa-let-7b	CDC2					
smad1-r-v	hsa-mir-139	SMAD1					
xiap-r-c	hsa-mir-140	KDR					
claudin-7-r-v	hsa-mir-511-2	CLDN7					
alpha-catenin-m-v	hsa-mir-1228	CTNNA1					
bim-r-v	hsa-mir-218-1	BCL2L11					
eef2k-r-v	hsa-mir-758	EEF2K					
ar-r-v	hsa-mir-452	AR					
ptch-r-c	hsa-mir-25	PTCH1					
p27-r-v	hsa-mir-758	CDKN1B					
c-kit-r-v	hsa-mir-22	KIT					
smad1-r-v	hsa-mir-377	SMAD1					
eef2k-r-v	hsa-mir-217	EEF2K					
her2-m-v	hsa-mir-511-1	ERBB2					
claudin-7-r-v	hsa-mir-24-1	CLDN7					
aib1-m-v	hsa-mir-139	NCOA3					
chk2-m-c	hsa-mir-485	CHEK2					
claudin-7-r-v	hsa-mir-758	CLDN7					
ar-r-v	hsa-mir-589	AR					
chk2-m-c	hsa-mir-140	CHEK2					
pcna-m-v	hsa-mir-132	PCNA					
setd2-r-na	hsa-mir-511-1	SETD2					
chk2-m-c	hsa-mir-223	CHEK2					
alpha-catenin-m-v	hsa-mir-605	CTNNA1					
claudin-7-r-v	hsa-mir-431	CLDN7					
irs1-r-v	hsa-mir-511-2	IRS1					
eef2k-r-v	hsa-mir-519a-2	EEF2K					
yb-1-r-v	hsa-mir-150	YBX1					
eef2k-r-v	hsa-mir-136	EEF2K					
pcna-m-v	hsa-mir-605	PCNA					
pcna-m-v	hsa-mir-485	PCNA					
xrcc1-r-c	hsa-mir-214	XRCC1					
pcna-m-v	hsa-mir-199a-1	PCNA					
eef2k-r-v	hsa-mir-432	EEF2K					
smad1-r-v	hsa-mir-214	SMAD1					
eef2k-r-v	hsa-mir-483	EEF2K					
c-kit-r-v	hsa-mir-511-1	KIT					
foxo3a-r-c	hsa-mir-142	FOXO3					
bim-r-v	hsa-mir-485	BCL2L11					
snail-m-c	hsa-mir-155	SNAI2					
er-alpha-r-v	hsa-mir-877	ESR1					
stat5-alpha-r-v	hsa-mir-605	STAT5A					
claudin-7-r-v	hsa-mir-654	CLDN7					
claudin-7-r-v	hsa-mir-337	CLDN7					
xrcc1-r-c	hsa-mir-1247	XRCC1					
claudin-7-r-v	hsa-mir-130b	CLDN7					
mre11-r-c	hsa-mir-766	MRE11A					

cdk1-r-v	hsa-mir-140	CDC2					
bim-r-v	hsa-mir-1976	BCL2L11					
gab2-r-v	hsa-mir-654	GAB2					
her2-m-v	hsa-mir-511-2	ERBB2					
chk2-m-c	hsa-mir-24-1	CHEK2					
eef2-r-v	hsa-mir-140	EEF2					
ar-r-v	hsa-mir-1976	AR					
pr-r-v	hsa-mir-31	PGR					
pkc-alpha-m-v	hsa-mir-511-2	PRKCA					
mre11-r-c	hsa-mir-511-2	MRE11A					
ku80-r-c	hsa-mir-217	XRCC5					
ku80-r-c	hsa-mir-24-1	XRCC5					
smac-m-v	hsa-mir-1249	DIABLO					
claudin-7-r-v	hsa-mir-370	CLDN7					
pcna-m-v	hsa-mir-511-1	PCNA					
bim-r-v	hsa-mir-409	BCL2L11					
eef2k-r-v	hsa-mir-455	EEF2K					
53bp1-r-c	hsa-mir-1295	TP53BP1					
xbp1-g-c	hsa-mir-223	XBP1					
er-alpha-r-v	hsa-mir-1276	ESR1					
dj-1-r-c	hsa-mir-140	PARK7					
syk-m-v	hsa-let-7e	SYK					
er-alpha-r-v	hsa-mir-1914	ESR1					
er-alpha-r-v	hsa-mir-605	ESR1					
smad1-r-v	hsa-mir-1247	SMAD1					
claudin-7-r-v	hsa-mir-181b-2	CLDN7					
pr-r-v	hsa-mir-629	PGR					
rab25-r-c	hsa-mir-223	RAB25					
yb-1-r-v	hsa-mir-1249	YBX1					
chk2-m-c	hsa-mir-1295	CHEK2					
xrcc1-r-c	hsa-mir-212	XRCC1					
gab2-r-v	hsa-mir-1247	GAB2					
e-cadherin-r-v	hsa-mir-1271	CDH1					
src-m-v	hsa-mir-142	SRC					
p53-r-v	hsa-mir-1908	TP53					
pkc-alpha-m-v	hsa-mir-511-1	PRKCA					
notch3-r-c	hsa-mir-365-2	NOTCH3					
p27-r-v	hsa-mir-487a	CDKN1B					
rab25-r-c	hsa-mir-511-2	RAB25					
rab25-r-c	hsa-mir-212	RAB25					
c-myc-r-c	hsa-mir-511-2	MYC					
xiap-r-c	hsa-mir-217	KDR					
smad1-r-v	hsa-mir-212	SMAD1					
msh6-r-c	hsa-mir-1249	MSH6					
ku80-r-c	hsa-mir-1249	XRCC5					
smad1-r-v	hsa-mir-487a	SMAD1					
eef2k-r-v	hsa-mir-370	EEF2K					
syk-m-v	hsa-mir-411	SYK					
rad50-m-c	hsa-mir-1295	RAD50					
eef2k-r-v	hsa-mir-181b-2	EEF2K					
caspase-8-m-c	hsa-mir-1247	CASP8					
gab2-r-v	hsa-mir-337	GAB2					
bim-r-v	hsa-mir-511-2	BCL2L11					
eef2k-r-v	hsa-mir-522	EEF2K					
bim-r-v	hsa-mir-145	BCL2L11					
p27-r-v	hsa-mir-181b-1	CDKN1B					
msh6-r-c	hsa-let-7a-2	MSH6					
msh6-r-c	hsa-let-7a-3	MSH6					
ptch-r-c	hsa-mir-223	PTCH1					
notch3-r-c	hsa-mir-511-2	NOTCH3					
src-m-v	hsa-mir-511-1	SRC					

jnk2-r-c	hsa-mir-217	MAPK9					
bak-r-c	hsa-mir-511-1	BAK1					
eif4e-r-v	hsa-mir-605	EIF4E					
claudin-7-r-v	hsa-mir-487b	CLDN7					
p53-r-v	hsa-mir-139	TP53					
p53-r-v	hsa-mir-140	TP53					
igf-1r-beta-r-c	hsa-mir-1228	IGF1R					
gab2-r-v	hsa-mir-134	GAB2					
eef2k-r-v	hsa-mir-369	EEF2K					
bcl-2-m-v	hsa-mir-210	BCL2					
caveolin-1-r-v	hsa-mir-551a	CAV1					
paxillin-r-v	hsa-mir-511-1	PXN					
yap-r-v	hsa-mir-1295	YAP1					
yap-r-v	hsa-mir-1228	YAP1					
smad1-r-v	hsa-mir-485	SMAD1					
p53-r-v	hsa-mir-589	TP53					
xiap-r-c	hsa-mir-485	KDR					
e-cadherin-r-v	hsa-mir-1306	CDH1					
pr-r-v	hsa-mir-1908	PGR					
inpp4b-g-c	hsa-mir-223	INPP4B					
smac-m-v	hsa-let-7b	DIABLO					
syk-m-v	hsa-mir-539	SYK					
pcna-m-v	hsa-mir-654	PCNA					
smad1-r-v	hsa-mir-605	SMAD1					
syk-m-v	hsa-mir-605	SYK					
smac-m-v	hsa-mir-140	DIABLO					
eef2k-r-v	hsa-mir-133a-1	EEF2K					
rab25-r-c	hsa-mir-142	RAB25					
claudin-7-r-v	hsa-mir-127	CLDN7					
akt-r-v	hsa-mir-217	AKT1	AKT2	AKT3			
bak-r-c	hsa-mir-511-2	BAK1					
aib1-m-v	hsa-mir-1247	NCOA3					
cdk1-r-v	hsa-mir-511-1	CDC2					
pea-15-r-v	hsa-mir-433	PEA15					
smac-m-v	hsa-mir-511-2	DIABLO					
gata3-m-v	hsa-mir-99b	GATA3					
inpp4b-g-c	hsa-mir-150	INPP4B					
53bp1-r-c	hsa-mir-589	TP53BP1					
c-kit-r-v	hsa-mir-551a	KIT					
mre11-r-c	hsa-mir-511-1	MRE11A					
igfbp2-r-v	hsa-mir-29c	IGFBP2					
er-alpha-r-v	hsa-mir-494	ESR1					
mek1-r-v	hsa-mir-1228	MAP2K1					
erk2-r-na	hsa-mir-511-1	MAPK1					
igf-1r-beta-r-c	hsa-mir-658	IGF1R					
53bp1-r-c	hsa-mir-146a	TP53BP1					
alpha-catenin-m-v	hsa-mir-1908	CTNNA1					
rad50-m-c	hsa-mir-511-1	RAD50					
yap-r-v	hsa-mir-217	YAP1					
bcl-2-m-v	hsa-mir-203	BCL2					
p53-r-v	hsa-mir-132	TP53					
caveolin-1-r-v	hsa-mir-130b	CAV1					
ku80-r-c	hsa-mir-605	XRCC5					
syk-m-v	hsa-mir-379	SYK					
c-kit-r-v	hsa-mir-15b	KIT					
gab2-r-v	hsa-mir-181a-1	GAB2					
dj-1-r-c	hsa-mir-342	PARK7					
bcl-x-r-c	hsa-mir-1295	BCL2L1					
pcna-m-v	hsa-mir-134	PCNA					
eef2k-r-v	hsa-mir-130b	EEF2K					
syk-m-v	hsa-mir-22	SYK					

igf-1r-beta-r-c	hsa-mir-203	IGF1R					
paxillin-r-v	hsa-mir-766	PXN					
e-cadherin-r-v	hsa-mir-329-1	CDH1					
pcna-m-v	hsa-mir-493	PCNA					
smac-m-v	hsa-mir-588	DIABLO					
smad1-r-v	hsa-mir-455	SMAD1					
rad50-m-c	hsa-mir-1247	RAD50					
inpp4b-g-c	hsa-mir-766	INPP4B					
p70s6k-r-v	hsa-mir-1247	RPS6KB1					
cdk1-r-v	hsa-mir-605	CDC2					
smac-m-v	hsa-mir-605	DIABLO					
smad1-r-v	hsa-mir-1228	SMAD1					
alpha-catenin-m-v	hsa-mir-214	CTNNA1					
Found by both the integrated model and the naïve model							
notch3-r-c	hsa-mir-150	NOTCH3			1	1	1
er-alpha-r-v	hsa-mir-18a	ESR1			1	1	1
p53-r-v	hsa-mir-150	TP53			1	1	
beta-catenin-r-v	hsa-mir-214	CTNNB1			1	1	
bim-r-v	hsa-mir-181a-1	BCL2L11			1	1	
igf-1r-beta-r-c	hsa-mir-223	IGF1R			1	1	
igf-1r-beta-r-c	hsa-mir-139	IGF1R			1	1	
p27-r-v	hsa-mir-181a-1	CDKN1B			1	1	
igf-1r-beta-r-c	hsa-mir-145	IGF1R			1	1	
smad3-r-v	hsa-mir-155	SMAD3			1	1	
msh6-r-c	hsa-mir-21	MSH6			1	1	
caveolin-1-r-v	hsa-mir-7-1	CAV1			1		1
bim-r-v	hsa-let-7a-2	BCL2L11			1		1
bim-r-v	hsa-let-7a-1	BCL2L11			1		1
bim-r-v	hsa-let-7a-3	BCL2L11			1		1
n-cadherin-r-v	hsa-mir-150	CDH2					1
yap-r-v	hsa-mir-150	YAP1					1
er-alpha-r-v	hsa-mir-766	ESR1					1
ku80-r-c	hsa-mir-223	XRCC5					1
beta-catenin-r-v	hsa-mir-223	CTNNB1					1
er-alpha-r-v	hsa-mir-493	ESR1					1
claudin-7-r-v	hsa-mir-214	CLDN7					1
e-cadherin-r-v	hsa-mir-605	CDH1					1
claudin-7-r-v	hsa-mir-1228	CLDN7					1
beta-catenin-r-v	hsa-mir-511-1	CTNNB1					1
er-alpha-r-v	hsa-mir-337	ESR1					1
er-alpha-r-v	hsa-mir-299	ESR1					1
bim-r-v	hsa-let-7b	BCL2L11					1
syk-m-v	hsa-mir-409	SYK					1
igf-1r-beta-r-c	hsa-mir-142	IGF1R					1
e-cadherin-r-v	hsa-mir-130b	CDH1					1
pcna-m-v	hsa-let-7a-2	PCNA					1
beta-catenin-r-v	hsa-mir-511-2	CTNNB1					1
syk-m-v	hsa-mir-654	SYK					1
e-cadherin-r-v	hsa-mir-493	CDH1					1
eef2k-r-v	hsa-mir-605	EEF2K					1
syk-m-v	hsa-mir-337	SYK					1
snail-m-c	hsa-mir-150	SNAI2					1
igf-1r-beta-r-c	hsa-mir-511-1	IGF1R					1
e-cadherin-r-v	hsa-mir-22	CDH1					1
er-alpha-r-v	hsa-mir-323	ESR1					1
er-alpha-r-v	hsa-mir-411	ESR1					1
bcl-2-m-v	hsa-mir-22	BCL2					1
er-alpha-r-v	hsa-mir-369	ESR1					1
e-cadherin-r-v	hsa-mir-654	CDH1					1
beta-catenin-r-v	hsa-mir-22	CTNNB1					1
n-cadherin-r-v	hsa-mir-511-1	CDH2					1

caveolin-1-r-v	hsa-mir-200a	CAV1					1
chk2-m-c	hsa-let-7b	CHEK2					1
akt-r-v	hsa-mir-223	AKT1	AKT2	AKT3			1
alpha-catenin-m-v	hsa-mir-142	CTNNA1					1
igf-1r-beta-r-c	hsa-mir-511-2	IGF1R					1
bim-r-v	hsa-mir-1295	BCL2L11					1
e-cadherin-r-v	hsa-mir-1908	CDH1					1
syk-m-v	hsa-mir-150	SYK					1
e-cadherin-r-v	hsa-mir-1228	CDH1					1
p70s6k-r-v	hsa-mir-511-2	RPS6KB1					1
c-myc-r-c	hsa-mir-486	MYC					1
b-raf-m-na	hsa-mir-145	BRAF					1
eef2k-r-v	hsa-mir-1247	EEF2K					1
igfbp2-r-v	hsa-mir-664	IGFBP2					1
p70s6k-r-v	hsa-mir-511-1	RPS6KB1					1
er-alpha-r-v	hsa-mir-1910	ESR1					1
eef2k-r-v	hsa-mir-487a	EEF2K					1
claudin-7-r-v	hsa-mir-493	CLDN7					1
e-cadherin-r-v	hsa-mir-511-2	CDH1					1
yap-r-v	hsa-mir-142	YAP1					1
akt-r-v	hsa-mir-511-2	AKT1	AKT2	AKT3			1
alpha-catenin-m-v	hsa-mir-223	CTNNA1					1
e-cadherin-r-v	hsa-mir-218-1	CDH1					1
akt-r-v	hsa-mir-766	AKT1	AKT2	AKT3			1
bim-r-v	hsa-mir-605	BCL2L11					1
yap-r-v	hsa-mir-605	YAP1					1
erk2-r-na	hsa-mir-223	MAPK1					1
beta-catenin-r-v	hsa-mir-146a	CTNNB1					1
caspase-8-m-c	hsa-mir-511-2	CASP8					1
syk-m-v	hsa-mir-541	SYK					1
er-alpha-r-v	hsa-mir-379	ESR1					1
chk2-m-c	hsa-let-7a-3	CHEK2					1
chk2-m-c	hsa-let-7a-2	CHEK2					1
e-cadherin-r-v	hsa-mir-511-1	CDH1					1
eef2k-r-v	hsa-mir-541	EEF2K					1
msh6-r-c	hsa-mir-142	MSH6					1
chk2-m-c	hsa-let-7a-1	CHEK2					1
e-cadherin-r-v	hsa-mir-299	CDH1					1
b-raf-m-na	hsa-mir-605	BRAF					1
c-met-m-c	hsa-mir-511-2	MET					1
fak-r-c	hsa-mir-616	PTK2					1
pkc-alpha-m-v	hsa-mir-150	PRKCA					1
bim-r-v	hsa-mir-223	BCL2L11					1
syk-m-v	hsa-mir-483	SYK					1
msh6-r-c	hsa-mir-146a	MSH6					1
b-raf-m-na	hsa-mir-223	BRAF					1
igfbp2-r-v	hsa-mir-29b-1	IGFBP2					1
b-raf-m-na	hsa-mir-511-2	BRAF					1
er-alpha-r-v	hsa-mir-218-1	ESR1					1
syk-m-v	hsa-mir-766	SYK					1
b-raf-m-na	hsa-mir-193a	BRAF					1
53bp1-r-c	hsa-let-7b	TP53BP1					1
caveolin-1-r-v	hsa-mir-616	CAV1					1
rb-m-v	hsa-mir-452	RB1					1
er-alpha-r-v	hsa-mir-199a-2	ESR1					1
caveolin-1-r-v	hsa-mir-200b	CAV1					1
c-met-m-c	hsa-mir-511-1	MET					1
jnk2-r-c	hsa-mir-223	MAPK9					1
chk1-r-v	hsa-mir-511-2	CHEK1					1
syk-m-v	hsa-mir-511-2	SYK					1
igf-1r-beta-r-c	hsa-mir-150	IGF1R					

beta-catenin-r-v	hsa-mir-150	CTNNB1					
e-cadherin-r-v	hsa-mir-214	CDH1					
53bp1-r-c	hsa-mir-150	TP53BP1					
alpha-catenin-m-v	hsa-mir-150	CTNNA1					
pr-r-v	hsa-mir-150	PGR					
ku80-r-c	hsa-mir-150	XRCC5					
claudin-7-r-v	hsa-mir-766	CLDN7					
xrcc1-r-c	hsa-mir-150	XRCC1					
e-cadherin-r-v	hsa-mir-1247	CDH1					
e-cadherin-r-v	hsa-mir-145	CDH1					
smad4-m-c	hsa-mir-150	SMAD4					
igfbp2-r-v	hsa-mir-224	IGFBP2					
eef2k-r-v	hsa-mir-766	EEF2K					
e-cadherin-r-v	hsa-mir-150	CDH1					
notch3-r-c	hsa-mir-146a	NOTCH3					
er-alpha-r-v	hsa-mir-541	ESR1					
smac-m-v	hsa-mir-150	DIABLO					
syk-m-v	hsa-mir-145	SYK					
er-alpha-r-v	hsa-mir-409	ESR1					
irs1-r-v	hsa-mir-150	IRS1					
er-alpha-r-v	hsa-mir-485	ESR1					
pr-r-v	hsa-mir-22	PGR					
e-cadherin-r-v	hsa-mir-766	CDH1					
syk-m-v	hsa-mir-377	SYK					
claudin-7-r-v	hsa-mir-1247	CLDN7					
syk-m-v	hsa-mir-214	SYK					
er-alpha-r-v	hsa-mir-134	ESR1					
er-alpha-r-v	hsa-mir-758	ESR1					
e-cadherin-r-v	hsa-mir-485	CDH1					
b-raf-m-na	hsa-mir-150	BRAF					
syk-m-v	hsa-mir-485	SYK					
er-alpha-r-v	hsa-mir-214	ESR1					
dj-1-r-c	hsa-mir-150	PARK7					
rad51-m-c	hsa-mir-150	RAD51					
er-alpha-r-v	hsa-mir-432	ESR1					
er-alpha-r-v	hsa-mir-377	ESR1					
er-alpha-r-v	hsa-mir-431	ESR1					
bim-r-v	hsa-mir-193a	BCL2L11					
gab2-r-v	hsa-mir-766	GAB2					
er-alpha-r-v	hsa-mir-487a	ESR1					
msh6-r-c	hsa-mir-1247	MSH6					
syk-m-v	hsa-mir-140	SYK					
pcna-m-v	hsa-mir-145	PCNA					
er-alpha-r-v	hsa-mir-433	ESR1					
notch3-r-c	hsa-mir-142	NOTCH3					
syk-m-v	hsa-mir-487a	SYK					
beta-catenin-r-v	hsa-mir-766	CTNNB1					
rad50-m-c	hsa-mir-150	RAD50					
pcna-m-v	hsa-mir-1295	PCNA					
er-alpha-r-v	hsa-mir-382	ESR1					
e-cadherin-r-v	hsa-mir-134	CDH1					
er-alpha-r-v	hsa-mir-370	ESR1					
alpha-catenin-m-v	hsa-mir-766	CTNNA1					
c-myc-r-c	hsa-mir-150	MYC					
e-cadherin-r-v	hsa-mir-139	CDH1					
rb-m-v	hsa-mir-150	RB1					
bcl-xl-r-c	hsa-mir-150	BCL2L1					
er-alpha-r-v	hsa-mir-483	ESR1					
msh6-r-c	hsa-mir-214	MSH6					
msh6-r-c	hsa-mir-1295	MSH6					
syk-m-v	hsa-mir-127	SYK					

er-alpha-r-v	hsa-mir-539	ESR1					
claudin-7-r-v	hsa-mir-605	CLDN7					
her2-m-v	hsa-mir-766	ERBB2					
her2-m-v	hsa-mir-150	ERBB2					
claudin-7-r-v	hsa-mir-485	CLDN7					
claudin-7-r-v	hsa-mir-217	CLDN7					
c-myc-r-c	hsa-mir-766	MYC					
chk2-m-c	hsa-mir-145	CHEK2					
er-alpha-r-v	hsa-mir-127	ESR1					
er-alpha-r-v	hsa-mir-654	ESR1					
e-cadherin-r-v	hsa-mir-409	CDH1					
syk-m-v	hsa-mir-758	SYK					
er-alpha-r-v	hsa-mir-136	ESR1					
syk-m-v	hsa-mir-132	SYK					
e-cadherin-r-v	hsa-mir-199a-1	CDH1					
igf-1r-beta-r-c	hsa-mir-766	IGF1R					
e-cadherin-r-v	hsa-mir-487a	CDH1					
bim-r-v	hsa-mir-150	BCL2L11					
ku80-r-c	hsa-mir-766	XRCC5					
er-alpha-r-v	hsa-mir-410	ESR1					
syk-m-v	hsa-mir-493	SYK					
e-cadherin-r-v	hsa-mir-199a-2	CDH1					
chk2-m-c	hsa-mir-150	CHEK2					
er-alpha-r-v	hsa-mir-1908	ESR1					
claudin-7-r-v	hsa-mir-541	CLDN7					
53bp1-r-c	hsa-mir-223	TP53BP1					
claudin-7-r-v	hsa-mir-204	CLDN7					
eif4e-r-v	hsa-mir-150	EIF4E					
p-cadherin-r-c	hsa-mir-150	CDH3					
smad1-r-v	hsa-mir-766	SMAD1					
pr-r-v	hsa-mir-605	PGR					
xrcc1-r-c	hsa-mir-223	XRCC1					
smad1-r-v	hsa-mir-145	SMAD1					
igfbp2-r-v	hsa-mir-452	IGFBP2					
53bp1-r-c	hsa-mir-766	TP53BP1					
igf-1r-beta-r-c	hsa-mir-589	IGF1R					
tau-m-c	hsa-mir-150	MAPT					
igfbp2-r-v	hsa-mir-150	IGFBP2					
e-cadherin-r-v	hsa-mir-204	CDH1					
cdk1-r-v	hsa-mir-150	CDC2					
pr-r-v	hsa-mir-223	PGR					
pr-r-v	hsa-mir-155	PGR					
syk-m-v	hsa-mir-433	SYK					
syk-m-v	hsa-mir-299	SYK					
e-cadherin-r-v	hsa-mir-377	CDH1					
e-cadherin-r-v	hsa-mir-212	CDH1					
chk1-r-v	hsa-mir-150	CHEK1					
b-raf-m-na	hsa-mir-1247	BRAF					
claudin-7-r-v	hsa-mir-487a	CLDN7					
syk-m-v	hsa-mir-134	SYK					
e-cadherin-r-v	hsa-mir-133a-1	CDH1					
rad50-m-c	hsa-mir-223	RAD50					
dvl3-r-v	hsa-mir-150	DVL3					
akt-r-v	hsa-mir-150	AKT1	AKT2	AKT3			
p27-r-v	hsa-mir-1276	CDKN1B					
e-cadherin-r-v	hsa-mir-199b	CDH1					
er-alpha-r-v	hsa-mir-130b	ESR1					
n-cadherin-r-v	hsa-mir-224	CDH2					
claudin-7-r-v	hsa-mir-1908	CLDN7					
e-cadherin-r-v	hsa-mir-1295	CDH1					
syk-m-v	hsa-mir-1295	SYK					

er-alpha-r-v	hsa-mir-496	ESR1					
igf-1r-beta-r-c	hsa-mir-1249	IGF1R					
syk-m-v	hsa-mir-432	SYK					
lck-r-v	hsa-mir-1269	LCK					
msh6-r-c	hsa-mir-605	MSH6					
msh6-r-c	hsa-mir-223	MSH6					
53bp1-r-c	hsa-mir-1247	TP53BP1					
notch3-r-c	hsa-mir-223	NOTCH3					
pr-r-v	hsa-mir-142	PGR					
bak-r-c	hsa-mir-150	BAK1					
e-cadherin-r-v	hsa-mir-152	CDH1					
syk-m-v	hsa-mir-1247	SYK					
dj-1-r-c	hsa-mir-766	PARK7					
er-alpha-r-v	hsa-mir-487b	ESR1					
igfbp2-r-v	hsa-mir-146a	IGFBP2					
53bp1-r-c	hsa-mir-1249	TP53BP1					
igf-1r-beta-r-c	hsa-mir-146a	IGF1R					
chk2-m-c	hsa-mir-1247	CHEK2					
msh6-r-c	hsa-mir-193a	MSH6					
igfbp2-r-v	hsa-mir-29a	IGFBP2					
53bp1-r-c	hsa-mir-511-2	TP53BP1					
eef2k-r-v	hsa-mir-485	EEF2K					
53bp1-r-c	hsa-mir-142	TP53BP1					
e-cadherin-r-v	hsa-mir-337	CDH1					
xrcc1-r-c	hsa-mir-140	XRCC1					
smac-m-v	hsa-mir-212	DIABLO					
beta-catenin-r-v	hsa-mir-1249	CTNNB1					
er-alpha-r-v	hsa-mir-543	ESR1					
xrcc1-r-c	hsa-mir-22	XRCC1					
foxo3a-r-c	hsa-mir-511-1	FOXO3					
syk-m-v	hsa-mir-410	SYK					
msh6-r-c	hsa-mir-140	MSH6					
xiap-r-c	hsa-mir-150	KDR					
claudin-7-r-v	hsa-mir-218-1	CLDN7					
bim-r-v	hsa-mir-1249	BCL2L11					
e-cadherin-r-v	hsa-mir-181b-2	CDH1					
gab2-r-v	hsa-mir-486	GAB2					
her2-m-v	hsa-mir-145	ERBB2					
lck-r-v	hsa-mir-149	LCK					
her2-m-v	hsa-mir-212	ERBB2					
lck-r-v	hsa-mir-1910	LCK					
53bp1-r-c	hsa-mir-605	TP53BP1					
beta-catenin-r-v	hsa-mir-1295	CTNNB1					
igf-1r-beta-r-c	hsa-mir-1247	IGF1R					
paxillin-r-v	hsa-mir-223	PXN					
er-alpha-r-v	hsa-mir-145	ESR1					
yap-r-v	hsa-mir-22	YAP1					
53bp1-r-c	hsa-mir-511-1	TP53BP1					
yap-r-v	hsa-mir-766	YAP1					
pr-r-v	hsa-mir-1228	PGR					
igf-1r-beta-r-c	hsa-mir-605	IGF1R					
e-cadherin-r-v	hsa-mir-758	CDH1					
ku80-r-c	hsa-mir-486	XRCC5					
smac-m-v	hsa-mir-1247	DIABLO					
b-raf-m-na	hsa-mir-214	BRAF					
her2-m-v	hsa-mir-223	ERBB2					
eef2k-r-v	hsa-mir-145	EEF2K					
syk-m-v	hsa-mir-487b	SYK					
syk-m-v	hsa-mir-382	SYK					
eef2k-r-v	hsa-mir-433	EEF2K					
e-cadherin-r-v	hsa-mir-432	CDH1					

e-cadherin-r-v	hsa-mir-382	CDH1					
syk-m-v	hsa-mir-431	SYK					
beta-catenin-r-v	hsa-mir-142	CTNNB1					
xbp1-g-c	hsa-mir-150	XBP1					
er-alpha-r-v	hsa-mir-1247	ESR1					
e-cadherin-r-v	hsa-mir-181a-1	CDH1					
rad50-m-c	hsa-mir-766	RAD50					
dvl3-r-v	hsa-mir-511-2	DVL3					
bim-r-v	hsa-mir-766	BCL2L11					
dvl3-r-v	hsa-mir-511-1	DVL3					
smad3-r-v	hsa-mir-22	SMAD3					
mek1-r-v	hsa-mir-149	MAP2K1					
beta-catenin-r-v	hsa-mir-224	CTNNB1					
chk2-m-c	hsa-mir-214	CHEK2					
smad4-m-c	hsa-mir-766	SMAD4					
e-cadherin-r-v	hsa-mir-455	CDH1					
notch3-r-c	hsa-mir-155	NOTCH3					
cd49b-m-v	hsa-mir-150	ITGA2					
er-alpha-r-v	hsa-mir-1228	ESR1					
claudin-7-r-v	hsa-mir-134	CLDN7					
b-raf-m-na	hsa-mir-766	BRAF					
notch3-r-c	hsa-mir-452	NOTCH3					
smac-m-v	hsa-mir-1295	DIABLO					
bim-r-v	hsa-mir-455	BCL2L11					
er-alpha-r-v	hsa-mir-99b	ESR1					
e-cadherin-r-v	hsa-mir-132	CDH1					
c-myc-r-c	hsa-mir-223	MYC					
msh6-r-c	hsa-mir-511-1	MSH6					
claudin-7-r-v	hsa-mir-483	CLDN7					
er-alpha-r-v	hsa-mir-486	ESR1					
xrcc1-r-c	hsa-mir-193a	XRCC1					
xrcc1-r-c	hsa-mir-145	XRCC1					
gab2-r-v	hsa-mir-605	GAB2					
claudin-7-r-v	hsa-mir-377	CLDN7					
eef2k-r-v	hsa-mir-539	EEF2K					
claudin-7-r-v	hsa-mir-1295	CLDN7					
er-alpha-r-v	hsa-mir-1224	ESR1					
p-cadherin-r-c	hsa-mir-24-1	CDH3					
rab25-r-c	hsa-mir-766	RAB25					
mek1-r-v	hsa-mir-766	MAP2K1					
bim-r-v	hsa-mir-214	BCL2L11					
claudin-7-r-v	hsa-mir-1306	CLDN7					
eef2-r-v	hsa-mir-150	EEF2					
msh6-r-c	hsa-mir-511-2	MSH6					
syk-m-v	hsa-mir-212	SYK					
syk-m-v	hsa-mir-133a-1	SYK					
smad4-m-c	hsa-mir-511-1	SMAD4					
igf-1r-beta-r-c	hsa-mir-339	IGF1R					
er-alpha-r-v	hsa-mir-329-1	ESR1					
chk2-m-c	hsa-mir-605	CHEK2					
e-cadherin-r-v	hsa-mir-433	CDH1					
smac-m-v	hsa-mir-766	DIABLO					
chk2-m-c	hsa-mir-766	CHEK2					
xrcc1-r-c	hsa-mir-452	XRCC1					
alpha-catenin-m-v	hsa-mir-1249	CTNNA1					
pr-r-v	hsa-mir-224	PGR					
notch3-r-c	hsa-mir-224	NOTCH3					
e-cadherin-r-v	hsa-let-7e	CDH1					
syk-m-v	hsa-mir-199a-1	SYK					
alpha-catenin-m-v	hsa-mir-1247	CTNNA1					
claudin-7-r-v	hsa-mir-99b	CLDN7					

xiap-r-c	hsa-mir-223	KDR					
bim-r-v	hsa-mir-486	BCL2L11					
caveolin-1-r-v	hsa-mir-425	CAV1					
yap-r-v	hsa-mir-511-2	YAP1					
claudin-7-r-v	hsa-mir-539	CLDN7					
foxo3a-r-c	hsa-mir-22	FOXO3					
dj-1-r-c	hsa-mir-511-1	PARK7					
xrcc1-r-c	hsa-mir-142	XRCC1					
e-cadherin-r-v	hsa-mir-539	CDH1					
igfbp2-r-v	hsa-mir-1249	IGFBP2					
igfbp2-r-v	hsa-mir-142	IGFBP2					
smad3-r-v	hsa-mir-511-2	SMAD3					
ku80-r-c	hsa-mir-511-2	XRCC5					
smad1-r-v	hsa-mir-150	SMAD1					
gab2-r-v	hsa-mir-181a-2	GAB2					
stat5-alpha-r-v	hsa-mir-218-1	STAT5A					
syk-m-v	hsa-mir-381	SYK					
eef2k-r-v	hsa-mir-150	EEF2K					
xrcc1-r-c	hsa-let-7b	XRCC1					
foxo3a-r-c	hsa-mir-486	FOXO3					
pkc-alpha-m-v	hsa-mir-223	PRKCA					
xiap-r-c	hsa-mir-1247	KDR					
4e-bp1-r-v	hsa-mir-1295	EIF4EBP1					
yap-r-v	hsa-mir-511-1	YAP1					
ku80-r-c	hsa-mir-1247	XRCC5					
b-raf-m-na	hsa-let-7b	BRAF					
xrcc1-r-c	hsa-mir-146a	XRCC1					
notch3-r-c	hsa-mir-616	NOTCH3					
caveolin-1-r-v	hsa-mir-182	CAV1					
nf2-r-c	hsa-mir-511-1	NF2					
ar-r-v	hsa-mir-511-2	AR					
claudin-7-r-v	hsa-mir-125a	CLDN7					
ku80-r-c	hsa-mir-511-1	XRCC5					
claudin-7-r-v	hsa-mir-1249	CLDN7					
n-cadherin-r-v	hsa-mir-588	CDH2					
mek1-r-v	hsa-mir-1249	MAP2K1					
yap-r-v	hsa-mir-1247	YAP1					
stat5-alpha-r-v	hsa-mir-455	STAT5A					
nf2-r-c	hsa-mir-511-2	NF2					
xrcc1-r-c	hsa-mir-217	XRCC1					
e-cadherin-r-v	hsa-mir-370	CDH1					
vasp-r-c	hsa-mir-504	VASP					
e-cadherin-r-v	hsa-mir-541	CDH1					
notch3-r-c	hsa-mir-22	NOTCH3					
bcl-xl-r-c	hsa-mir-140	BCL2L1					
her2-m-v	hsa-mir-1247	ERBB2					
gab2-r-v	hsa-mir-377	GAB2					
p53-r-v	hsa-mir-766	TP53					
er-alpha-r-v	hsa-mir-154	ESR1					
rad50-m-c	hsa-mir-217	RAD50					
er-alpha-r-v	hsa-mir-1295	ESR1					
msh6-r-c	hsa-mir-139	MSH6					
alpha-catenin-m-v	hsa-mir-145	CTNNA1					
e-cadherin-r-v	hsa-mir-486	CDH1					
p27-r-v	hsa-mir-1254	CDKN1B					
syk-m-v	hsa-mir-370	SYK					
pr-r-v	hsa-mir-181a-1	PGR					
e-cadherin-r-v	hsa-mir-891a	CDH1					
er-alpha-r-v	hsa-mir-181b-2	ESR1					
dj-1-r-c	hsa-mir-1295	PARK7					
igf-1r-beta-r-c	hsa-let-7i	IGF1R					

smac-m-v	hsa-mir-214	DIABLO					
claudin-7-r-v	hsa-mir-133a-1	CLDN7					
paxillin-r-v	hsa-mir-1249	PXN					
n-cadherin-r-v	hsa-mir-140	CDH2					
53bp1-r-c	hsa-mir-145	TP53BP1					
p-cadherin-r-c	hsa-mir-23b	CDH3					
xrcc1-r-c	hsa-mir-511-1	XRCC1					
igf-1r-beta-r-c	hsa-mir-1976	IGF1R					
beta-catenin-r-v	hsa-mir-212	CTNNB1					
p27-r-v	hsa-mir-541	CDKN1B					
er-alpha-r-v	hsa-mir-1306	ESR1					
bcl-xl-r-c	hsa-mir-145	BCL2L1					
smac-m-v	hsa-mir-145	DIABLO					
irs1-r-v	hsa-mir-24-1	IRS1					
syk-m-v	hsa-mir-199a-2	SYK					
pr-r-v	hsa-mir-766	PGR					
pea-15-r-v	hsa-mir-511-2	PEA15					
syk-m-v	hsa-mir-496	SYK					
bak-r-c	hsa-mir-766	BAK1					
beta-catenin-r-v	hsa-mir-605	CTNNB1					
e-cadherin-r-v	hsa-mir-574	CDH1					
er-alpha-r-v	hsa-mir-329-2	ESR1					
foxo3a-r-c	hsa-mir-212	FOXO3					
eif4e-r-v	hsa-mir-1249	EIF4E					
p27-r-v	hsa-mir-99b	CDKN1B					
igfbp2-r-v	hsa-let-7f-1	IGFBP2					
notch3-r-c	hsa-mir-1266	NOTCH3					
pea-15-r-v	hsa-mir-511-1	PEA15					
mek1-r-v	hsa-mir-296	MAP2K1					
dj-1-r-c	hsa-mir-409	PARK7					
caveolin-1-r-v	hsa-mir-375	CAV1					
53bp1-r-c	hsa-mir-1228	TP53BP1					
53bp1-r-c	hsa-mir-24-1	TP53BP1					
ku80-r-c	hsa-mir-1228	XRCC5					
er-alpha-r-v	hsa-mir-212	ESR1					
beta-catenin-r-v	hsa-mir-217	CTNNB1					
bcl-xl-r-c	hsa-mir-212	BCL2L1					
her2-m-v	hsa-mir-217	ERBB2					
53bp1-r-c	hsa-mir-22	TP53BP1					
p27-r-v	hsa-mir-1307	CDKN1B					
bcl-2-m-v	hsa-mir-511-2	BCL2					
notch3-r-c	hsa-let-7i	NOTCH3					
igfbp2-r-v	hsa-let-7b	IGFBP2					
notch3-r-c	hsa-mir-511-1	NOTCH3					
er-alpha-r-v	hsa-mir-139	ESR1					
lck-r-v	hsa-mir-99b	LCK					
53bp1-r-c	hsa-mir-224	TP53BP1					
gab2-r-v	hsa-mir-539	GAB2					
syk-m-v	hsa-mir-543	SYK					
pten-r-v	hsa-mir-766	PTEN					
pea-15-r-v	hsa-mir-1910	PEA15					
xrcc1-r-c	hsa-mir-224	XRCC1					
cdk1-r-v	hsa-mir-217	CDC2					
caveolin-1-r-v	hsa-mir-429	CAV1					
nf2-r-c	hsa-mir-150	NF2					
gab2-r-v	hsa-mir-455	GAB2					
chk2-m-c	hsa-mir-139	CHEK2					
yap-r-v	hsa-mir-1249	YAP1					
4e-bp1-r-v	hsa-mir-145	EIF4EBP1					
gab2-r-v	hsa-mir-541	GAB2					
e-cadherin-r-v	hsa-mir-1249	CDH1					

mek1-r-v	hsa-mir-504	MAP2K1					
claudin-7-r-v	hsa-mir-891a	CLDN7					
jnk2-r-c	hsa-mir-150	MAPK9					
cdk1-r-v	hsa-mir-664	CDC2					
gab2-r-v	hsa-mir-1910	GAB2					
caveolin-1-r-v	hsa-mir-96	CAV1					
setd2-r-na	hsa-mir-223	SETD2					
igfbp2-r-v	hsa-mir-223	IGFBP2					
4e-bp1-r-v	hsa-mir-605	EIF4EBP1					
msh6-r-c	hsa-mir-217	MSH6					
bcl-x-r-c	hsa-mir-181a-1	BCL2L1					
b-raf-m-na	hsa-mir-1249	BRAF					
igf-1r-beta-r-c	hsa-mir-24-1	IGF1R					
e-cadherin-r-v	hsa-mir-217	CDH1					
igfbp2-r-v	hsa-mir-101-2	IGFBP2					
e-cadherin-r-v	hsa-mir-431	CDH1					
n-cadherin-r-v	hsa-mir-193a	CDH2					
cdk1-r-v	hsa-mir-511-2	CDC2					
ku80-r-c	hsa-mir-142	XRCC5					
caveolin-1-r-v	hsa-mir-210	CAV1					
xrcc1-r-c	hsa-mir-766	XRCC1					
igf-1r-beta-r-c	hsa-mir-486	IGF1R					
dj-1-r-c	hsa-mir-22	PARK7					
caveolin-1-r-v	hsa-mir-141	CAV1					
cdk1-r-v	hsa-mir-29a	CDC2					
e-cadherin-r-v	hsa-mir-342	CDH1					
syk-m-v	hsa-mir-1228	SYK					
beta-catenin-r-v	hsa-mir-133a-1	CTNNB1					
nf2-r-c	hsa-mir-129-2	NF2					
msh6-r-c	hsa-mir-377	MSH6					
syk-m-v	hsa-mir-584	SYK					
her2-m-v	hsa-mir-1249	ERBB2					
chk2-m-c	hsa-mir-133a-1	CHEK2					
dvl3-r-v	hsa-mir-766	DVL3					
p27-r-v	hsa-mir-486	CDKN1B					
gab2-r-v	hsa-mir-485	GAB2					
xrcc1-r-c	hsa-mir-365-2	XRCC1					
smad3-r-v	hsa-mir-223	SMAD3					
e-cadherin-r-v	hsa-mir-487b	CDH1					
notch3-r-c	hsa-mir-365-1	NOTCH3					
smac-m-v	hsa-mir-1228	DIABLO					
caspase-8-m-c	hsa-mir-99b	CASP8					
irs1-r-v	hsa-mir-223	IRS1					
alpha-catenin-m-v	hsa-mir-212	CTNNA1					
gab2-r-v	hsa-mir-431	GAB2					
cdk1-r-v	hsa-mir-125a	CDC2					
jnk2-r-c	hsa-mir-140	MAPK9					
c-myc-r-c	hsa-mir-217	MYC					
mek1-r-v	hsa-mir-24-1	MAP2K1					
vegfr2-r-c	hsa-mir-551a	KDR					
setd2-r-na	hsa-mir-140	SETD2					
rab25-r-c	hsa-mir-217	RAB25					
xrcc1-r-c	hsa-mir-139	XRCC1					
53bp1-r-c	hsa-mir-214	TP53BP1					
lck-r-v	hsa-mir-605	LCK					
gab2-r-v	hsa-mir-487a	GAB2					
er-alpha-r-v	hsa-mir-381	ESR1					
ku80-r-c	hsa-mir-146a	XRCC5					
53bp1-r-c	hsa-mir-217	TP53BP1					
smac-m-v	hsa-mir-224	DIABLO					
er-alpha-r-v	hsa-mir-140	ESR1					

msh6-r-c	hsa-mir-574	MSH6					
bcl-x-r-c	hsa-mir-212	BCL2L1					
n-cadherin-r-v	hsa-mir-522	CDH2					
rad51-m-c	hsa-mir-217	RAD51					
4e-bp1-r-v	hsa-mir-193a	EIF4EBP1					
notch3-r-c	hsa-mir-505	NOTCH3					
igf-1r-beta-r-c	hsa-mir-212	IGF1R					
foxo3a-r-c	hsa-mir-140	FOXO3					
eef2k-r-v	hsa-mir-223	EEF2K					
her2-m-v	hsa-mir-584	ERBB2					
setd2-r-na	hsa-mir-217	SETD2					
p27-r-v	hsa-mir-144	CDKN1B					
Found by naïve model only							
akt-r-v	hsa-mir-146b	AKT1	AKT2	AKT3	1		
chk1-r-v	hsa-mir-511-1	CHEK1					1
alpha-catenin-m-v	hsa-mir-140	CTNNA1					1
vasp-r-c	hsa-mir-1276	VASP					1
paxillin-r-v	hsa-mir-505	PXN					1
pten-r-v	hsa-mir-511-2	PTEN					1
bcl-x-r-c	hsa-mir-1276	BCL2L1					1
bim-r-v	hsa-mir-132	BCL2L11					
claudin-7-r-v	hsa-mir-1258	CLDN7					
aib1-m-v	hsa-mir-511-2	NCOA3					
p21-r-c	hsa-mir-25	CDKN1A					
aib1-m-v	hsa-mir-511-1	NCOA3					
rad50-m-c	hsa-mir-132	RAD50					
c-myc-r-c	hsa-mir-541	MYC					
tau-m-c	hsa-mir-144	MAPT					
ar-r-v	hsa-mir-190	AR					
c-raf-r-v	hsa-mir-190	RAF1					
alpha-catenin-m-v	hsa-mir-217	CTNNA1					
c-myc-r-c	hsa-mir-140	MYC					
rad51-m-c	hsa-mir-140	RAD51					
er-alpha-r-v	hsa-mir-150	ESR1					
lck-r-v	hsa-mir-129-2	LCK					
aib1-m-v	hsa-mir-190	NCOA3					
her2-m-v	hsa-mir-139	ERBB2					
vasp-r-c	hsa-mir-184	VASP					

were found only by the integrated model, were confirmed by miRanda database. However, only 6 targets found by the naïve model only were confirmed by miRanda database. MirTarbase, a dataset based on manually surveying pertinent literature [23] was used to further verify our results. 15 suggested targets found by both the integrated and the naïve model were supported by the MirTarBase dataset. 11 of the 15 suggested targets found by both the integrated and the naïve model were supported by strong experimental evidences according to the MirTarBase dataset. One suggested target found by the integrated model only were supported by strong experimental evidences according to the MirTarBase dataset. None of the suggested targets found by the naïve model only were supported by strong experimental evidences according to the MirTarBase dataset. This suggests that there could be a number of undiscovered miRNA targets included in the findings of integrated and naïve models. The list of 822 miRNA/protein pairs was included in the appendix (Table A3).

Discussion

The traditional way to detect direct targets of miRNA using miRNA-mRNA experiment method is limited, due to the fact that miRNAs may regulate their targets post-transcriptionally. In addition, other computational methods, which were based on optimal sequence complementarity of miRNA and mRNA, suffer from large percentage of false positives and of limited practical use. Taking the advantage of recent technique advance in measuring of miRNA expression and protein concentration levels in a high-throughput scale, we proposed to search for potential miRNA targets through a nonlinear hierarchical model. Computationally, this integrated model measures the correlation between miRNA and its targeting protein without making estimation of protein expression levels first as in the naïve method. We used both simulation studies and an application to the real data to compare our proposed method and the naïve method. Our simulation results suggested that both integrated and naïve methods can well control their type-I errors, however, the integrated method consistently showed higher detection powers than the naïve method under different scenarios, particularly when the protein intensity values were located close to the saturation point or the background noise level. In the real data example, our proposed integrated method detected much more potential miRNA targets than the naïve method. Furthermore, the number of potential miRNA targets, which can be confirmed by computational methods or literatures, is larger in the integrated method than that in the naïve method.

A significant association between a miRNA/protein pair can be

either direct or indirect. For example, a miRNA may directly target and degrade a transcription factor (TF), which in turn induces indirect cascading effects of down-regulating the TF's target genes. The association analyses from the simple or our integrated model would reveal both direct and indirect associations. In contrast, the other computer-based algorithms, e.g. miRanda, can only predict direct miRNA targets based on sequence comparison. In the real data analyses (Table 1), the relatively smaller percentage of overlap between our findings and miRanda database suggests that our algorithm may detect more indirect targets. This is sound since our algorithm is more powerful, as demonstrated by our simulation studies, and hence is capable of detecting smaller indirect associations. With the cross-reference to miRanda database, those direct miRNA targets of more biological relevance could be filtered out to serve as top candidates for further biological validations. It is worth noting that our algorithm can indeed detect more direct miRNA targets in absolute number. Also, in Table 1, the results were based on a FDR of 10% for the multiple test adjustment; however, we also checked a FDR at 5% level and found the conclusion remained the same. That is, the proposed integrated method found more miRNA targets that appear in other existing databases, demonstrating its advantage over the naïve method.

Unknown parameters in our proposed model were estimated within the maximum likelihood framework. Using the asymptotic properties of maximum likelihood estimates, test statistics were straightforward to construct. However, some improvement can be made to further improve the proposed model. For example, we assumed a linear relationship between miRNA and protein to directly compare with the naïve method and to illustrate our model using simple examples, but in reality, the relationship between miRNAs and proteins could follow a nonlinear relationship, such as a dose-response curve. In this case, (z_i) can be replaced by other parametric or nonparametric functions. With some simple modifications, our model can be easily extended to relax these assumptions. Additionally, in this article the random error terms for different dilution steps were set to be independent and identically distributed as proposed in other RPPA analysis papers [10]. However, it is possible that the errors may be highly correlated. In this case, more complicated dependence matrix among serial dilution steps can also be readily incorporated into our model framework.

References

1. Pritchard CC, Cheng HH, Tewari M (2012) MicroRNA profiling: approaches and considerations. Nat Rev Genet 13: 358-369.
2. Tang G, Reinhart BJ, Bartel DP, Zamore PD (2003) A biochemical framework for RNA silencing in plants. Genes Dev 17: 49-63.
3. Xie Z, Kasschau KD, Carrington JC (2003) Negative feedback regulation of Dicer-Like1 in Arabidopsis by microRNA-guided mRNA degradation. Curr Biol 13: 784-789.
4. Doench JG, Sharp PA (2004) Specificity of microRNA target selection in translational repression. Genes Dev 18: 504-511.
5. Zeng Y, Wagner EJ, Cullen BR (2002) Both natural and designed micro RNAs can inhibit the expression of cognate mRNAs when expressed in human cells. Mol Cell 9: 1327-1333.
6. Betel D, Koppal A, Agius P, Sander C, Leslie C (2010) Comprehensive modeling of microRNA targets predicts functional non-conserved and non-canonical sites. Genome Biol 11: R90.
7. Lewis BP, Shih IH, Jones-Rhoades MW, Bartel DP, Burge CB (2003) Prediction of mammalian microRNA targets. Cell 115: 787-798.
8. Brennecke J, Stark A, Russell RB, Cohen SM (2005) Principles of microRNA-target recognition. PLoS Biol 3: e85.
9. Mueller C, Liotta LA, Espina V (2010) Reverse phase protein microarrays advance to use in clinical trials. Mol Oncol 4: 461-481.
10. Tabus I, Hategan A, Mircean C, Rissanen J, Shmulevich I, et al. (2006). Nonlinear modeling of protein expressions in protein arrays. IEEE Transactions on Signal Processing 54: 2394-2407.
11. Yang JY, He X (2011) A multistep protein lysate array quantification method and its statistical properties. Biometrics 67: 1197-1205.
12. Hu J, He X, Baggerly KA, Coombes KR, Hennessy BT, et al. (2007) Non-parametric quantification of protein lysate arrays. Bioinformatics 23: 1986-1994.
13. Gelman A, Chew GL, Shnaidman M (2004) Bayesian analysis of serial dilution assays. Biometrics 60: 407-417.
14. Golub G, Pereyra V (2003) Separable nonlinear least squares: the variable projection method and its applications. Inverse problems, 19: R1.
15. Pinheiro JC, Bates DM (1995) Approximations to the log-likelihood function in the nonlinear mixed-effects model. Journal of Computational and Graphical Statistics 4: 12-35.
16. Lindstrom MJ, Bates DM (1988) Newton-Raphson and EM algorithms for linear mixed-effects models for repeated-measures data. Journal of the American Statistical Association, 83: 1014-1022.
17. Dennis Jr JE, Schnabel RB (1996) Numerical methods for unconstrained optimization and nonlinear equations. Classics in Applied Mathematics CL16: xv + 375.
18. Benjamini Y, Hochberg Y (1995) Controlling the false discovery rate: a practical and powerful approach to multiple testing. J R Statist Soc 57: 289-300.
19. Enright AJ, John B, Gaul U, Tuschl T, Sander C, et al. (2003) MicroRNA targets in Drosophila. Genome Biol 5: R1.
20. Hofacker IL, Fontana W, Stadler PF, Bonhoeffer LS, Tacker M, et al. (1994). Fast folding and comparison of RNA secondary structures. Monatshefte für Chemie/Chemical Monthly 125: 167-188.
21. Zuker M, Stiegler P (1981) Optimal computer folding of large RNA sequences using thermodynamics and auxiliary information. Nucleic Acids Res 9: 133-148.
22. McCaskill JS (1990) The equilibrium partition function and base pair binding probabilities for RNA secondary structure. Biopolymers 29: 1105-1119.
23. Hsu SD, Tseng YT, Shrestha S, Lin YL, Khaleel A, et al. (2014) miRTarBase update 2014: an information resource for experimentally validated miRNA-target interactions. Nucleic Acids Res 42: D78-85.